NASA TECHNICAL NOTE

NASA TN D-4740

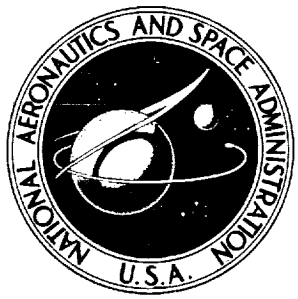

NASA TN D-4740

ATTITUDE DETERMINATION OF THE SPIN-STABILIZED PROJECT SCANNER SPACECRAFT

by T. M. Walsh, Jean C. Keating, and Dwayne E. Hinton

Langley Research Center
Langley Station, Hampton, Va.

NATIONAL AERONAUTICS AND SPACE ADMINISTRATION • WASHINGTON, D. C. • AUGUST 1968

NASA TN D-4740

ATTITUDE DETERMINATION OF THE SPIN-STABILIZED PROJECT SCANNER SPACECRAFT

By T. M. Walsh, Jean C. Keating,
and Dwayne E. Hinton

Langley Research Center
Langley Station, Hampton, Va.

NATIONAL AERONAUTICS AND SPACE ADMINISTRATION

For sale by the Clearinghouse for Federal Scientific and Technical Information
Springfield, Virginia 22151 – CFSTI price $3.00

CONTENTS

ATTITUDE DETERMINATION OF THE SPIN-STABILIZED PROJECT SCANNER SPACECRAFT

By T. M. Walsh, Jean C. Keating,
and Dwayne E. Hinton
Langley Research Center

SUMMARY

The Scanner experiment required continuous knowledge of the spacecraft celestial attitude with a one-sigma accuracy of 0.016°. The basic measurements used to obtain attitude information were sighting times of stars viewed by the star mapper on the Project Scanner vehicle. Each star sighting produced coded-pulse sequences the amplitudes of which were related to the visual magnitude of the star. The times of occurrences of these pulse sequences were related to the angular separation between a pair of stars. These angular-separation data were used to identify the sighted stars.

The right ascension and declination of the identified stars and their transit times were used to identify the values of a set of parameters in an assumed model of the vehicle dynamical equations of motion. These vehicle motion parameters were then used to determine the vehicle celestial attitude as a function of time.

A brief discussion of the star mapper is presented and the technique used to detect transit times of stars from the coded signals of the star mapper is described. A complete description of the star identification and parameter identification procedures is presented. A preflight analysis, used to establish predicted accuracies of attitude determination, is described. The estimated accuracies of vehicle attitude and star-mapper optical-axis pointing direction for Project Scanner flights 1 and 2 are discussed. The estimated one-sigma error in pointing direction of the star-mapper optical axis for these two flights was 0.006°; this value compared favorably with the experimental requirement of 0.016°.

INTRODUCTION

Langley Research Center has been engaged in a series of experiments designed to obtain flight measurements of the infrared radiance signature of the earth's horizon. (See ref. 1.) The intent of these experiments is to provide necessary basic information to design and evaluate infrared horizon sensors which utilize the earth's limb or horizon for spacecraft attitude-measurement purposes. Project Scanner was designed to obtain high resolution measurements of the earth's horizon radiance profile in two infrared

spectral intervals and to position these measurements accurately with respect to the solid earth. The Scanner experiment was flown on a suborbital ballistic rocket vehicle fired from Wallops Island, Virginia. The first flight was made on August 16, 1966, and the second, on December 10, 1966.

An operational schematic of the Scanner spacecraft is shown in figure 1. The spacecraft was despun to approximately 3/4 revolution per second when horizon data-gathering altitude was reached, and was erected to within 2° of the local vertical by a cold gas reaction jet control system similar to that described in reference 2. Two radiometers, each having a basic resolution of 0.025°, were mounted back to back in the spacecraft. Radiometer 1 was used to sense radiance in the 14- to 16-micron or carbon dioxide region and radiometer 2 was used to sense radiance in the 20- to 35-micron or water vapor region. The fields of view of the radiometers were scanned through the horizon at 10° per second by motor-driven mirrors. Precise attitude and submissile point information was needed to position the infrared radiance measurements at earth geographical locations. The geographical position of the spacecraft submissile point was determined with the aid of standard radar tracking techniques. Celestial attitude information was obtained by means of the star mapper in the Scanner vehicle (ref. 3) which was used to detect star transits as the star-mapper field of view was scanned through the celestial sphere by the spacecraft spin. All spacecraft data were transmitted to earth on a real-time basis for data processing and later combined with ground tracking data for reconstruction of the measured earth infrared horizon profiles. This report is concerned primarily with a description of the data obtained from the star mapper and the data processing necessary to determine the spacecraft celestial attitude. Related discussions are presented to show the development of the data-reduction accuracy criteria and the results of application of the data processing to flight data.

SYMBOLS

A,B,C	transformation matrices
a	estimated azimuthal separation of a pair of observed stars, degrees
d_1,d_2	earth radii, kilometers
e_k	estimated elevation angle of kth observed star in star-mapper field of view, degrees
F	a matrix of first partial derivatives of JDEHR with respect to each undetermined element of $\underline{X}$

F_{lm}	an element of matrix F
G_1,G_2	any two stars of celestial sphere (fig. 11)
g_c	angular separation of a pair of stars based on cataloged star positions, degrees
g_o	estimated angular separation of a pair of stars based on star-mapper data, degrees
Δg	allowable difference in angular separation of cataloged stars and estimated angular separation of observed stars, degrees
h	spacecraft altitude, kilometers
h_t	tangent height, kilometers
I_1,I_2,I_3	spacecraft moments of inertia, slug-ft^2
$\hat{i},\hat{j},\hat{k}$	unit vectors with subscripts denoting specific frames (fig. 6)
J,D,E,H	transformation matrices (table III)
M	tolerance limit on convergence of correction vector $\Delta\underline{X}$
m_v	apparent visual magnitude of a star
Q_k^j	jth estimate of quadratic form of error in k star sightings based on vector $\underline{r}$
$\underline{R}$	unit vector to a star in celestial reference frame
$\underline{r}$	unit vector to a star in a slit plane reference frame
r_l	an element of unit vector $\underline{r}$
T	time duration of a star transit across narrowest reticle slit, seconds
t	time, seconds

t_k	observed kth star transit time, seconds
t_{Sk}, t_{Vk}	observed star transit time of slanted and vertical slit planes, seconds
t_k^t	true kth star transit time, seconds
t_ν	a specific instant of time, seconds
Δt_k	kth time residual, seconds
V	matrix multiplier of modified vector of undetermined parameters, $\Delta\underline{Y}$
$\underline{X}$	vector of undetermined parameters
$\underline{\tilde{X}}^j$	jth estimate of vector of undetermined parameters
$\Delta\underline{X}$	correction vector of undetermined parameters
$\Delta\underline{X}^j$	jth estimate of $\Delta\underline{X}$
x_m	an element of vector of m undetermined parameters
Δx_m	an element of correction vector $\Delta\underline{X}$
$\Delta\underline{Y}$	modified correction vector of undetermined parameters
Δy	element of modified correction vector $\Delta\underline{Y}$
α, δ	right ascension and declination, respectively, degrees
β	rotation of a slit plane with respect to a plane perpendicular to an arbitrary azimuthal plane, degrees
β_1, β_2	rotation of slanted and vertical slit planes, respectively, with respect to a plane perpendicular to test table azimuthal plane, degrees
β_S, β_V	rotation of slanted and vertical slit planes, respectively, with respect to a plane perpendicular to star-mapper azimuthal plane, degrees

γ azimuthal displacement of any slit plane from optical axis, degrees

γ_S, γ_V azimuthal displacement of slanted and vertical slit planes from optical axis, degrees

ϵ_1, ϵ_2 misalinement angles of vehicle principal spin axis relative to star-mapper reference frame, degrees

ϵ_{tk} simulated kth star transit time error, seconds

$\epsilon_\alpha(t)_6, \epsilon_\delta(t)_6$ time history of pointing-direction error of vehicle principal spin axis in right ascension and declination, respectively, degrees

$\epsilon_\alpha(t)_8, \epsilon_\delta(t)_8$ time history of pointing-direction error of optical axis in right ascension and declination, respectively, degrees

η star elevation angle in any slit plane, degrees

η_S, η_V star elevation angle in slanted and vertical slit planes, respectively, degrees

θ, ϕ, ψ Euler angles defining orientation of vehicle principal axis relative to an inertial reference frame, degrees

Θ, Φ Euler angles defining the position of vehicle angular momentum vector in celestial reference frame, degrees

μ angular width of narrowest reticle slit, degrees

σ_a standard deviation of pointing-direction error of any selected axis, degrees

$\sigma_a(t_\nu)_6, \sigma_a(t_\nu)_8$ simulation results of standard deviation of pointing-direction error of vehicle principal axis and optical axis at specific instants of time, degrees

$\sigma_a(t_\nu)_{max}$ maximum standard deviation of pointing-direction error of optical axis at specific instant of time for simulated data, degrees

σ_t standard deviation of time errors used with simulated data, seconds

σ_{tr} standard deviation of time residuals for simulated or flight data, seconds

$\sigma_{\alpha}(t_{\nu})_6$ standard deviation of pointing-direction error of vehicle principal axis in right ascension for a specific instant of time of simulated data, degrees

$\sigma_{\alpha}(t_{\nu})_8$ standard deviation of pointing-direction error of optical axis in right ascension for a specific instant of time of simulated data, degrees

ϕ_o, ψ_o initial values of ϕ and ψ, degrees

ω total spin rate of vehicle principal spin axis, degrees/second

ω_{est} estimate of ω from raw star-mapper signals, degrees/second

Subscript:

k integer

Superscripts:

T matrix transpose

-1 matrix inverse

Derivatives with respect to time are denoted by dots over the variable. An underline denotes a vector, a ~ denotes an estimated value and ^ denotes a unit vector.

PROBLEM DESCRIPTION

The experimental requirement of locating the earth's horizon radiance profiles relative to the solid earth can be best expressed in terms of locating a radiometer line of sight relative to an earth radius. This relationship is shown in figure 2 where the radiometer line of sight is shown displaced from the solid earth by a distance h_t defined as the tangent height. The spacecraft is indicated at an altitude h, and the earth's radius is indicated by the radii d_1 and d_2. The Scanner experiment required that the measured radiance profiles be located relative to the solid earth with a one-sigma accuracy of 1.5 kilometers for a spacecraft altitude of 1100 kilometers. This accuracy requirement may be expressed in terms of an angular accuracy in positioning of the radiometer line of sight as 0.022^o. The significant error sources which affect this accuracy are: errors in radar tracking of the spacecraft altitude and submissile point, uncertainties in the

radiometer scan mirror position measurements, uncertainties in the knowledge of the alinement between the star mapper and radiometer, and inaccuracies in the celestial attitude determination from using star-mapper information. The contributions of all error sources excluding celestial attitude errors were estimated to be 0.015°. The allowable tangent height error due to errors in celestial-attitude determination was determined by assuming that all tangent height errors were independent and that their root-sum-square value was equal to the total allowable error expressed in degrees. By using this assumption, the allowable one-sigma error in spacecraft celestial attitude determination by using star-mapper information was computed to be 0.016°. Past experience with the difficulties in achieving the theoretical design limits of attitude-measurement systems by using complex optical devices led to the more conservative design goal of an allowable one-sigma error of 0.006° in spacecraft celestial attitude determination.

The measurements used to obtain attitude information were provided by a passively scanning star telescope called a star mapper, which is described in detail in reference 3. The star mapper is shown mounted in the spacecraft in figure 1. The instrument used a refractive optical system based on a modified Petzval design with a 15-inch (38.1 cm) focal length, a 5-inch (12.7 cm) clear aperture, and a field of view of 6° by 6°. The instrument-mounting positioned the star-mapper optical axis normal to the expected principal spin axis of the spacecraft. A coded reticle, shown in figure 3, was centered in the focal plane of the instrument, and a photo detector was placed behind the reticle. The reticle was principally opaque and contained a pair of identically coded sequences of transparent slits, one vertical group and one slanted group. The narrowest slit had a resolution of 0.015°. The coding feature of the reticle was used to reduce the system response to noise and to the multitude of stars dimmer than a threshold visual magnitude; this feature was selected to insure a minimum of three detectable and identifiable stars per vehicle spin period. (See ref. 4.) Spin motion of the spacecraft caused star images to travel across the reticle and produced two coded sequences of radiant energy which were sensed by the photo detector and transmitted to a ground receiving station. The ground-received coded star signals were tape recorded simultaneously with range time signals having a 10-microsecond resolution.

The procedures involved in determining celestial attitude of the Scanner vehicle from this raw data tape are illustrated in figure 4. Processing of the recorded star signals consisted of four major operations: time detection of apparent star sightings; manual pairing of star sighting times to reduce the number of false star sightings; identification of detected stars; and identification of the parameters of the dynamical equations of motion describing the spacecraft attitude. A brief description of the first two operations, which are discussed in reference 3, is presented herein for clarity, and the latter two operations are discussed in detail in this report.

TIME DETECTION AND MANUAL SORTING OF APPARENT STAR SIGHTINGS

As shown in figure 4, the recorded coded star-mapper signals were compared with a threshold level and all signals exceeding this threshold were converted to a digital signal with a star presence in a slit designated by a 1 and a star absence in a slit designated by a zero. Ideally, a nine-element code pattern of 110100010 would result from a passage of a single star across each group of slits. The last code element of 0 was added arbitrarily to a single code group to provide a return to zero voltage condition at the termination of each code group. The time duration T of a star signal generated by a star transit across the narrowest transparent slit was set by

$$T = \frac{\mu}{\omega_{est}}$$

where μ is 0.015^{o} for each element of the nine-element code and the estimated spin rate ω_{est} was determined from examination of an oscillograph record of the raw star-mapper data in which time periods between repeated sightings of the more prominent star signals were assumed to be the time period for a complete vehicle spin cycle.

The sample time used in the analog-to-digital converter was selected to be $T/4$ in microseconds. The presence of a star in a single element was indicated when two or more of four consecutive sample time intervals had signal levels which exceeded the variable threshold level. The uncertainty in the time of occurrence of a star presence or a star absence signal was $T/2$ microseconds. The output of the analog-to-digital converter was cross correlated in the decoder with a prestored replica of a code group as illustrated in figure 5. A star transit time t_k was acknowledged when correlation of the reference code sequence with any nine-element coded sequence produced agreement of at least two of four 1's and all five 0's or at least three of four 1's and at least four of five 0's. The transit times of apparent stars were recorded $T/4$ microseconds after the time of occurrence of the trailing edge of the ninth code element. The delay time of $T/4$ microseconds was necessary for readout of range time. The total uncertainty in star transit time included the ± 5-microsecond uncertainty in range time and $\pm T/2$-microsecond uncertainty in the time of occurrence of a star presence or star absence signal.

At this point, a distinction must be made between the physical groups of slits on the actual reticle and the analytical slit edges for which star transit times are defined. A transit time, recorded by the correlator as the time at which a star transits some point fixed with respect to the reticle, corresponds to a line on the reticle located 9.25μ after the leading edge of the vertical or slanted groups of slits. The analytical lines on the reticle described by 9.25μ after the leading edge of the vertical and slanted slit groups are defined to lie in planes designated as the vertical and slanted slit planes, respectively. A geometrical description of these slit planes is discussed in a later section.

The output of the correlator was a listing of apparent star transit times and their signal amplitudes. This listing was hand sorted in an attempt to relate transit times to discrete star sightings. The listing was examined for pairs of coded sequences of approximately equal amplitude such as a single star's transit of the field of view would be expected to produce. This amplitude sorting was repeated for all vehicle spin cycles as determined from the estimated vehicle spin rate. Additional sorting was done by searching for a recurrence of approximately equal time intervals between a pair of pulse sequences produced by the same star and the recurrence of approximately equal time intervals between pairs of sequences produced by different stars. The star-mapper data were then listed in the form of a pair of transit times for each apparent star sighting.

STAR AND PARAMETER IDENTIFICATION

The two primary operations of the star-mapper data processing procedure shown in figure 4 are the identification of the detected stars and the identification of the parameters of the dynamical equations of motion describing the spacecraft attitude. The listing of star transit time pairs was operated upon in a star identification program which produced a listing of identified stars and their sighting times. The identified star listing was used as input data to a parameter identification program, its resulting output being a set of the parameters which defines the dynamical equations of motion of the spacecraft. A priori data were used in both the star and parameter identification programs in the form of estimates of nominal vehicle trajectory, vehicle moments of inertia based on preflight measurements, and an approximation of vehicle spin rate based on successive sightings of identified stars. The following sections describe in detail the spacecraft attitude geometry, the mathematical model assumed for the dynamical equations of motion, the star identification program, and the parameter identification program.

Space Attitude Geometry

The general problem considered here is one of a geometrical formulation of the celestial attitude of a reference frame fixed in a spinning, torque-free, prolate, symmetrical, rigid body. The problem is further defined as one for which the orientation of the body-fixed reference is to be defined at instants of time at which known stars are observed and as a function of time for periods during which no stars are observed. The basic measurements which are used to determine vehicle orientations are the times at which known stars appear in the transit slit planes of the star-mapper reticle.

Basic reference frames.- The geometrical model for this problem involves the use of eight basic reference frames. Two additional reference frames were used to allow for star-mapper mounting misalinements and uncertainties in relationship of the vehicle principal axis to the vehicle body axes. The sequence of rotations and transformation

matrices for the defined Euler angles are listed in table I. The reference frames used in the solution are (see fig. 6):

(1) Celestial reference frame with unit vectors $\hat{i}_1,\hat{j}_1,\hat{k}_1$. The unit vectors $\hat{i}_1$ and $\hat{k}_1$ are selected to be in the direction of the first point of Aries and the North celestial pole, respectively. The unit vector $\hat{j}_1$ is selected to lie in the celestial equatorial plane to complete a right-hand system.

(2) Inertial reference frame defined by two Euler angles Φ and Θ relative to the celestial reference frame. In this frame the unit vector $\hat{k}_3$ is defined as parallel to the angular momentum vector of the spacecraft.

(3) A body-fixed reference frame defined by the Euler angles ϕ, θ, and ψ relative to the inertial reference frame. In this frame the unit vectors $\hat{i}_6$, $\hat{j}_6$, and $\hat{k}_6$ are defined to be parallel to the principal axes of the body. The unit vector $\hat{k}_6$ is defined to be along the vehicle spin axis. Since the vehicle is assumed to be symmetrical, the unit vectors $\hat{i}_6$ and $\hat{j}_6$ may be selected to be any mutually orthogonal pair which is also orthogonal to $\hat{k}_6$. For convenience, the $\hat{i}_6$ vector is considered to be directed along the nominal optical axis of the star mapper.

(4) The reference frame of the star mapper relative to the spacecraft principal axes is defined by two misalinement Euler angles ϵ_1 and ϵ_2. These two angles allow for misalinement of the star-mapper system relative to the spacecraft spin axis as measured prior to launch and also allow for changes in the location of true spin axis after launch and rocket fuel burnout. In this reference frame the $\hat{i}_8$ vector is selected to be along the optical axis of the star mapper.

(5) The last reference frame of interest is defined by the location of the vertical and slanted slit planes (in which star transit times are detected) relative to the star-mapper optical reference frame. Two Euler angles γ and β define this frame relative to the optical frame. There are actually two sets of γ and β; one set defines the vertical (γ_V,β_V) and the other, the slanted (γ_S,β_S) slit planes. In either case the $\hat{i}_{10}$ and $\hat{k}_{10}$ unit vectors are defined to be in the vertical or slanted slit plane.

One additional angle is needed to complete the geometrical formulation of the problem. This angle defines the coordinates of a star as sighted in a slit-plane reference frame. Figure 7 is a representation of a slit plane and the angles γ and β relative to the optical axis of the star mapper. In this figure a star sighting is shown in the slit plane at an angle η relative to the intersection of the $\hat{i}_8 - \hat{j}_8$ and $\hat{i}_{10} - \hat{k}_{10}$ planes. A unit vector to a star sighted in the slit-plane reference frame is

$$\underline{r} = \cos\eta\hat{i}_{10} + 0\hat{j}_{10} + \sin\eta\hat{k}_{10} \tag{1}$$

Figure 8 illustrates the geometry of the problem. For simplicity, the angles ϵ_1, ϵ_2, β_V, γ_V, β_S, γ_S, η_V, and η_S are not shown.

Preflight determination of β and γ.- The optical axis of the star mapper was defined by a small transparent square called the alinement point, located in the center of the reticle. The relationship of this alinement point to the two groups of coded slits and to the radiometers and the azimuthal separation between the leading and trailing edges of both the vertical and the slanted slit groups were established by preflight measurements. These measurements were used to determine the four angles referred to as the slit parameter angles, β_V, β_S, γ_V, and γ_S. A discussion of the techniques used to obtain these preflight measurements is given in reference 3. A geometrical application of these measurements to the determination of the slit parameter angles is given in appendix A of this report. These angles are illustrated by the schematic of the reticle given in figure 9. The total angular relationship between the two groups of slits, defined by the angle β, was determined. The angles β_V and β_S were defined as follows:

$$\beta_V = 0$$

$$\beta_S = \beta$$

As stated previously, the transit time pairs represent a known star's transit of points fixed with respect to the reticle. Schematically, these points lie on each of two analytical lines located on the reticle 9.25μ after the leading edge of the vertical and slanted groups of slits. These two analytical lines were designated as the vertical slit plane and the slanted slit plane. The azimuthal angular relationships of the optical axis to these two analytical slits were defined by the angles γ_V and γ_S as shown in figure 9.

Vehicle dynamics.- The relationship between the coordinates of an identified star in the celestial reference frame and the coordinate of the star as sighted in a slit-plane reference frame may be determined by use of the defined Euler angular rotations:

$$\underline{R} = (\Phi)(\Theta)(\phi)(\theta)(\psi)(\epsilon_1)(\epsilon_2)(\gamma)(\beta)\underline{r} \tag{2}$$

The vector $\underline{R}$ may also be written as

$$\underline{R} = \cos\alpha\cos\delta\hat{i}_1 + \sin\alpha\cos\delta\hat{j}_1 + \sin\delta\hat{k}_1 \tag{3}$$

where α and δ are the right ascension and declination of the identified star. The vector $\underline{r}$ has previously been defined (eq. (1)) as

$$\underline{r} = \cos\eta\hat{i}_{10} + 0\hat{j}_{10} + \sin\eta\hat{k}_{10}$$

where η is defined as the elevation angle of the star in a slit plane. For the case of a spinning torque-free symmetrical rigid body, the angles ϕ and ψ of equation (2) are defined as

$$\phi = \dot{\phi}t + \phi_o \tag{4}$$

$$\psi = \dot{\psi}t + \psi_o \tag{5}$$

and the rates $\dot{\phi}$ and $\dot{\psi}$ are defined as in reference 5.

$$\dot{\phi} = \frac{I_3\omega}{I_1 \cos\theta} \tag{6}$$

$$\dot{\psi} = \frac{(I_1 - I_3)\omega}{I_1} \tag{7}$$

where I_3 is the moment of inertia about the principal spin axis of the vehicle; I_1 is the moment of inertia about either one of a pair of axes which are mutually orthogonal and orthogonal to the principal spin axis of the body; and ω is the total spin velocity about the principal spin axis of the body.

If all parameters of equation (2) were uniquely defined, the attitude of any set of axes would be known. However, only the γ and β angles of equation (2) were assumed to be well known before flight. Of the remaining parameters in equation (2), ϵ_1, ϵ_2, θ, ϕ_o, and ψ_o were assumed to be unknown; estimates of Φ and Θ were available from launch data; and estimates of ω, $\dot{\phi}$, and $\dot{\psi}$ were available from preliminary examination of star-mapper data. With the use of identified stars, their sighting times, and least-square techniques, the parameters of equation (2) were identified. A summary of all a priori estimates based on preflight measurements and raw star-mapper data which were used in processing the data from Scanner flights 1 and 2 are listed in table II.

Star Identification

A star identification program was used to identify each star associated with each pair of transit times detected in the decoding routine. One of the primary requirements of the program was that the transit times be in chronological order and that the times appear in pairs, each pair being from the same star. The equatorial coordinates of the reference stars used in this program were obtained from the Boss catalog (ref. 6) and updated to the nearest 0.1 day of the time of flight by use of the astronomical techniques described in reference 7. The reference star listing was reduced by elimination from consideration all stars dimmer than a visual magnitude of +3.5 (ref. 3). The star listing was further reduced by selecting all stars falling within a selected band of the celestial sphere. The limits of this band, shown as an extended field of view in figure 10, were

defined to have the zenith angles of 76° and 104° away from the direction of spacecraft angular momentum vector as estimated from launch data. This band of $\pm 14^{\circ}$ about the spacecraft equator was necessary to accommodate the $\pm 3^{\circ}$ field of view of the star mapper, an uncertainty of $\pm 5^{\circ}$ in the estimated angular momentum direction, and a possible 6° vehicle cone angle.

All stars of the reduced reference list were considered as candidates for the transiting stars. An additional listing of all these candidate stars was made in the form of a catalog of angular separation g_c of each pair of stars in the reference list. Star identification was principally a process of finding a cataloged angular separation which agreed to within a fixed tolerance Δg of an estimated angular separation g_o of a pair of observed stars.

Angular separation of cataloged stars.- The angular separations of the cataloged stars are easily determined from their equatorial coordinates. In figure 11, the position of star G_1 on the celestial sphere is defined by coordinates (α_1,δ_1) and the position of star G_2 is defined by the coordinates (α_2,δ_2). The angular separation between G_1 and G_2, defined by arc G_1G_2 and designated as g_c, is given by law of cosines for spherical triangles as:

$$\cos g_c = \sin \delta_1 \sin \delta_2 + \cos \delta_1 \cos \delta_2 \cos(\alpha_1 - \alpha_2) \tag{8}$$

Angular separation of observed stars.- The angular separation between a pair of observed stars was estimated by use of the times at which the two stars transited the two slits of the reticle. This estimation was based on the assumption that vehicle cone angle and the misalinement angles were zero. These assumptions led directly to the definition of the azimuth-angle separation of a pair of stars as observed by the star mapper; that is,

$$a = \omega_{est}\left(t_{V(k+1)} - t_{Vk}\right) \tag{9}$$

where ω_{est} is the a priori estimated total spin rate and the subscripts k and V indicate the kth star transit of the vertical slit plane. The azimuthal separation of two observed stars as defined in equation (9) is analogous to the difference in the right ascension angles of two cataloged stars as shown in figure 11. The elevation angle e_k of a single star as observed by the star mapper may be written in a manner similar to that of equation (A4) in appendix A as

$$\tan e_k = \frac{\sin\left[\omega_{est}(t_{Sk} - t_{Vk}) - (|\gamma_V| + |\gamma_S|)\right]}{\tan \beta_S} \tag{10}$$

where the subscripts Sk and Vk refer to the kth star transit of the slanted slit plane and the vertical slit plane, respectively. The estimated total angular separation g_o of a pair of observed stars may be written in the identical form of equation (8) as

$$\cos g_o = \sin e_k \sin e_{k+1} + \cos e_k \cos e_{k+1} \cos a \tag{11}$$

A pair of stars in the reference list was selected as the prime candidate for the identification of a pair of observed stars if

$$\left| g_c - g_o \right| \leq \Delta g \tag{12}$$

where Δg is some fixed allowable difference in the two angular separations. This difference was adjustable and was set to be that value which would result in the selection of a sufficient number of prime candidate star pairs so that at least three stars per vehicle spin period were identified. Positive identification of sighted stars was accomplished by identifying triplets of sighted stars by using the procedures discussed in appendix B.

After star-identification processing was completed for one spin period, all information related to the identified stars was available. This information included the Boss catalog number, visual magnitude, right ascension, and declination of each identified star. The information also included a listing of transit times of each identified star for both the vertical and slanted slit planes. Each succeeding spin period was treated in a similar manner with no knowledge from previous spin periods assumed, since the flight data were expected to contain a minimum of three stars per spin period. After processing was completed for all spin periods, a synopsis made of all stars identified and the pertinent information for each star was printed. These data were next used in the parameter determination program.

Parameter Identification

In the development of the spacecraft-attitude determination geometry, equation (2) was derived to show the relationship between the celestial coordinates of an identified star and the coordinates of the star in either the vertical or slanted slit plane reference frames. Substituting equations (1) and (3) into equation (2) results in

$$\begin{pmatrix} \cos \delta \cos \alpha \\ \cos \delta \sin \alpha \\ \sin \delta \end{pmatrix} = (\Phi)(\Theta)(\phi)(\theta)(\psi)(\epsilon_1)(\epsilon_2)(\gamma)(\beta) \begin{pmatrix} \cos \eta \\ 0 \\ \sin \eta \end{pmatrix} \tag{13}$$

The parameters ϕ and ψ have been previously defined (eqs. (4) and (5)) as

$$\phi = \dot{\phi} t + \phi_o$$

$$\psi = \dot{\psi} t + \psi_o$$

The nine undetermined parameters of equation (13) are Φ, Θ, $\dot{\phi}$, ϕ_o, θ, $\dot{\psi}$, ψ_o, ϵ_1, ϵ_2. An observed star will produce two equations such as equation (13), one each for the

slanted and vertical slit planes. If an adequate number of stars are observed, an iterative method may be used to solve for the undetermined parameters of equation (13). Since a large number of star observations were expected, a least-squares technique was selected for solution of the undetermined parameters.

Equation (13) may be rewritten as $\underline{r} = JDEH\underline{R}$, where

$$\left.\begin{aligned} D &= (\epsilon_2)^{-1}(\epsilon_1)^{-1} \\ E &= (\psi)^{-1}(\theta)^{-1}(\phi)^{-1} \\ H &= (\Theta)^{-1}(\Phi)^{-1} \\ J &= (\beta)^{-1}(\gamma)^{-1} \end{aligned}\right\} \tag{14}$$

The individual elements of the matrices J, D, E, and H are given in table III. The dependence of $\underline{r}$ on the undetermined parameters may be expressed in functional form as

$$\underline{r}(\underline{X}) = JDEH\underline{R} \tag{15}$$

where $\underline{X}$ is defined as the column vector of undetermined parameters

$$\underline{X} = \begin{pmatrix} \theta \\ \psi_o \\ \dot{\psi} \\ \phi_o \\ \dot{\phi} \\ \Phi \\ \Theta \\ \epsilon_1 \\ \epsilon_2 \end{pmatrix} \tag{16}$$

The dependence of $\underline{r}$ on γ and β is implied in equation (15), but these parameters were not included in the vector $\underline{X}$ since they were assumed to be well known before flight. The vector function $\underline{r}$ may be expanded about the true values of $\underline{X}$ by use of a Taylor series expansion as

$$\underline{r}(\underline{X}) \approx \underline{r}(\underline{X} - \Delta\underline{X}) + F(\underline{X} - \Delta\underline{X})\Delta\underline{X} \tag{17}$$

In equation (17) all terms higher than the first variational terms are assumed to be negligible. The matrix F is the matrix of first partial derivatives of the elements of $\underline{r}(\underline{X})$ with respect to each element of $\underline{X}$ and evaluated at $\underline{X} - \Delta\underline{X}$. Each element of F is expressed as

$$F_{lm} = \frac{\partial r_l}{\partial x_m} \tag{18}$$

where

$$l = 1, 2, 3$$

and

$$m = 1, 2, 3, \ldots 9$$

The vector $\underline{X} - \Delta\underline{X}$ represents an estimate of $\underline{X}$, and $\Delta\underline{X}$ represents the error in the estimate. This estimate of $\underline{X}$ is denoted by $\tilde{\underline{X}}$ hereafter. From the jth estimate for $\underline{X}$, or $\tilde{\underline{X}}^{(j)}$, and k star transit times, equation (17) may be written as a set of k equations

$$\underline{r}(\underline{X})_k \approx \underline{r}\left(\tilde{\underline{X}}^{(j)}\right)_k + F\left(\tilde{\underline{X}}^{(j)}\right)_k \Delta\underline{X}^{(j)} \tag{19}$$

The dimensions of the vectors and matrices in equation (19) are

$$\underline{r}(\underline{X})_k \rightarrow 3k \times 1$$

$$\underline{r}\left(\tilde{\underline{X}}^{(j)}\right)_k \rightarrow 3k \times 1$$

$$F\left(\tilde{\underline{X}}^{(j)}\right)_k \rightarrow 3k \times m \qquad (k = 1, 2, 3, \ldots, k)$$

$$\Delta\underline{X}^{j} \rightarrow m \times 1$$

If the error in the approximation of the set of k equations represented by equation (19) is defined as $Q_k^{(j)}$,

$$Q_k^{(j)} = \underline{r}\left(\tilde{\underline{X}}^{(j)}\right)_k - \underline{r}(\underline{X})_k + F\left(\tilde{\underline{X}}^{(j)}\right)_k \Delta\underline{X}^{(j)} \tag{20}$$

The quadratic form of the error is

$$Q_k^{(j)T} Q_k^{(j)} = \left[\underline{r}\left(\tilde{\underline{X}}^{(j)}\right)_k - \underline{r}(\underline{X})_k\right]^T \left[\underline{r}\left(\tilde{\underline{X}}^{(j)}\right)_k - \underline{r}(\underline{X})_k\right] + \left[\underline{r}\left(\tilde{\underline{X}}^{(j)}\right)_k - \underline{r}(\underline{X})_k\right]^T F\left(\tilde{\underline{X}}^{(j)}\right)_k \Delta\underline{X}^{(j)}$$

$$+ \Delta\underline{X}^{(j)T} F\left(\tilde{\underline{X}}^{(j)}\right)_k^T \left[\underline{r}\left(\tilde{\underline{X}}^{(j)}\right)_k - \underline{r}(\underline{X})_k\right] + \Delta\underline{X}^{(j)T} F\left(\tilde{\underline{X}}^{(j)}\right)_k^T F\left(\tilde{\underline{X}}^{(j)}\right)_k \Delta\underline{X}^{(j)} \tag{21}$$

By using the usual method of a least-squares solution, the quadratic form of the error is minimized by setting its partial derivative with respect to each member of $\Delta\underline{X}$ equal to zero for all m or

$$\frac{\partial}{\partial \Delta x_m} Q_k^{(j)^T} Q_k^{(j)} = 0 = F\left(\tilde{\underline{X}}^{(j)}\right)_k^T \left[\underline{r}\left(\tilde{\underline{X}}^{(j)}\right)_k - \underline{r}(\underline{X})_k\right] + F\left(\tilde{\underline{X}}^{(j)}\right)_k^T F\left(\tilde{\underline{X}}^{(j)}\right)_k \Delta\underline{X}^{(j)} \tag{22}$$

There are nine equations such as equation (22), one for each of the undetermined parameters. The error vector $\Delta\underline{X}^{(j)}$ may be determined from equation (22) as

$$\Delta\underline{X}^{(j)} = -\left[F\left(\tilde{\underline{X}}^{(j)}\right)_k^T F\left(\tilde{\underline{X}}^{(j)}\right)_k\right]^{-1} F\left(\tilde{\underline{X}}^{(j)}\right)_k^T \left[\underline{r}\left(\tilde{\underline{X}}^{(j)}\right)_k - \underline{r}(\underline{X})_k\right] \tag{23}$$

A new estimate of $\underline{X}$ may now be determined as

$$\tilde{\underline{X}}^{(j+1)} = \tilde{\underline{X}}^{(j)} + \Delta\underline{X}^{(j)} \tag{24}$$

where $\tilde{\underline{X}}^{(j)}$ is the jth estimate of $\underline{X}$ and $\Delta\underline{X}^{(j)}$ is the solution to equation (23). This solution is based on a knowledge of the variable elevation angle η in each slit for each star transit. Since the elevation angle was variable and not measurable, an alternate formulation of the problem was desirable for simplicity of problem solution.

Examination of equation (13) shows that there are two independent equations for each star transit time. Also each observed star results in a pair of transit times and a pair of independent equations for the slanted and vertical slit plane transits. If the parameters of equation (13) were known, the equations for the slanted slit plane transit could be predicted based on a solution of the equations resulting from the vertical slit plane transit time. This condition means that knowledge of η_V implies knowledge of η_S and this condition further implies that only two independent equations exist for each pair of star transit times. The problem solution can therefore be simplified by making use of the constraint equation represented by the second element of equation (13). Applying this constraint to equation (15) results in

$$0 = J_2 DEH\underline{R} \tag{25}$$

where the subscript 2 on J refers to the second row of the matrix J. Applying the previously described method to equation (25) results in a new definition of the correction vector

$$\Delta\underline{X}^{(j)} = \left\{\left[F_2\left(\tilde{\underline{X}}^{(j)}\right)_k\right]^T \left[F_2\left(\tilde{\underline{X}}^{(j)}\right)_k\right]\right\}^{-1} \left[F_2\left(\tilde{\underline{X}}^{(j)}\right)_k\right]^T \underline{r}_2\left(\tilde{\underline{X}}^{(j)}\right)_k \tag{26}$$

where the subscript 2 refers to the second row of matrix F and the second element of the vector $\underline{r}$. Dimensions of the matrices in equation (26) are

$$\Delta\underline{X}^{(j)} \rightarrow m \times 1$$

$$F_2\left(\tilde{\underline{X}}^{(j)}\right)_k \rightarrow k \times m$$

$$\underline{r}_2\left(\tilde{\underline{X}}^{(j)}\right)_k \rightarrow k \times 1$$

As before (eq. (24)), a new estimate for $\underline{X}$ may be obtained by

$$\tilde{\underline{X}}^{(j+1)} = \tilde{\underline{X}}^{(j)} + \Delta\underline{X}^{(j)}$$

where $\tilde{\underline{X}}^{(j)}$ is the old estimate and $\Delta\underline{X}^{(j)}$ is the solution to equation (26). The updating of the estimates of $\underline{X}$ may be continued until each element of $\Delta\underline{X}^{(j)} \leq M$, where M is a predetermined convergence criteria based on the required accuracy of convergence.

If either or both of the parameters θ and Θ are zero, the matrix

$$\left[F_2\left(\tilde{\underline{X}}^{(j)}\right)_k\right]^T\left[F_2\left(\tilde{\underline{X}}^{(j)}\right)_k\right]$$

of equation (26) is singular and no solution for $\Delta\underline{X}$ is possible. If these two parameters are nonzero, but nearly zero, the matrix is nearly singular and special care must be taken to invert this matrix. In the case of the Scanner vehicle launchings, the angle Θ was never less than 50^o and therefore presented no problem. However, the vehicle cone angle θ was expected to be less than 6^o and special treatment was necessary for inversion of the matrix. A discussion of the inversion procedure is presented in appendix C.

Initial Estimates of $\underline{X}$

Before a solution of the values of the nine undetermined parameters of $\underline{X}$ is possible, initial estimates are needed. These initial estimates were obtained by considering a reduced problem of the three undetermined parameters $\psi_o + \phi_o$, Φ, and Θ. By assuming θ, ϵ_1, and ϵ_2 to be zero, $\dot{\phi}$ and $\dot{\psi}$ were calculated by use of ω_{est} and the preflight measured values of I_1 and I_3. The values of Θ and Φ used to initiate this solution were estimated from launch data. The initial estimate of $\phi_o + \psi_o$ for the three-unknown problem was determined by using equation (13) with the assumption that γ_V was zero, and setting the vertical slit transit time of the first identified star to be zero. In addition, the elevation angle η_V was assumed to be zero. Equation (13) then becomes

$$\begin{pmatrix} \cos\delta\cos\alpha \\ \cos\delta\sin\alpha \\ \sin\delta \end{pmatrix} = (\Phi)(\Theta)(\phi_o)(\psi_o)\begin{pmatrix} 1 \\ 0 \\ 0 \end{pmatrix} \tag{27}$$

By making use of the definitions of the transformation matrices listed in table I, equation (27) becomes

$$\begin{pmatrix} \cos\delta_1\cos\alpha_1 \\ \cos\delta_1\sin\alpha_1 \\ \sin\delta_1 \end{pmatrix} = \begin{pmatrix} \cos\Phi & -\cos\Theta\sin\Phi & \sin\Theta\sin\Phi \\ \sin\Phi & \cos\Theta\cos\Phi & -\sin\Theta\cos\Phi \\ 0 & \sin\Theta & \cos\Theta \end{pmatrix}\begin{pmatrix} \cos(\phi_o + \psi_o) \\ \sin(\phi_o + \psi_o) \\ 0 \end{pmatrix} \tag{28}$$

where the subscript on α and δ denotes the right ascension and declination values of the first observed star. The matrix equation (28) may be solved for $\phi_o + \psi_o$ as

$$\tan(\phi_o + \psi_o) = \frac{-\cos\delta_1\cos\Theta\sin(\Phi - \alpha_1) + \sin\Theta\sin\delta_1}{\cos\delta_1\cos(\Phi - \alpha_1)} \tag{29}$$

In this three-unknown problem, the $\Delta\underline{Y}$ correction vector as defined in appendix C becomes

$$\Delta\underline{Y} = \begin{pmatrix} 0 \\ \Delta y_2 \\ 0 \\ \Delta y_4 \\ \Delta y_5 \\ 0 \\ 0 \\ 0 \\ 0 \end{pmatrix} \tag{30}$$

where the elements Δy_2, Δy_4, and Δy_5 were computed by the least-squares program discussed previously. The solution for $\underline{X}$ resulting from this procedure produced an initial estimate for $\psi_o + \phi_o$ and better estimates for Φ and Θ which were then applied to the problem of the nine undetermined parameters. This approach produced satisfactory estimates of the sum of ψ_o and ϕ_o, but no knowledge of estimates of their individual values. The procedure used here was arbitrarily to set $\phi_o = \psi_o = \frac{\psi_o + \phi_o}{2}$ as initial estimates for the nine-unknown problem. This procedure is a reasonable one

since the solution of the nine-unknown problem is heavily dependent on $\phi_0 + \psi_0$ and lightly dependent on their individual values for a small cone angle as discussed in appendix C. A summary of all a priori estimates is listed in table II. These a priori estimates were used to initiate the three-unknown problem.

DEVELOPMENT OF DATA-REDUCTION ACCURACY CRITERIA FROM PREFLIGHT ANALYSIS

Before application of the attitude determination technique to flight-data reduction the accuracy of the parameter identification method had to be ascertained in order to establish expected accuracies for the Project Scanner flights. In addition, criteria had to be developed in order to assess the adequacy of any estimate of $\underline{X}$ as determined from flight data. To establish the expected accuracy of spacecraft attitude determination, a simulation study was performed. Criteria for assessing the adequacy of estimates of $\underline{X}$ were developed by using the results of this study. In this study simulated flight data were generated by using the expected launch and flight conditions of Project Scanner flight 1. The mathematical model of simulated spacecraft equations of motion was identical to that which was assumed for the flight vehicle. Simulated flight data were in the form of a time list of transited stars and the right ascension and declination values of these stars updated to the expected launch time. These simulated data were used to estimate the values of the previously described parameters of the vector $\underline{X}$ in the same manner as for flight data. The parameters of $\underline{\tilde{X}}$ were used to generate pointing-direction time histories of selected axes. The errors in these pointing directions, specifically the pointing-direction errors of the optical axis, were the basis of assessing the accuracy of the attitude determination solution.

Pointing-Direction Analysis

Figure 12 shows a flow diagram illustrating the generation of time histories used in the simulation studies. A set of nine parameters defining the equations of motion, launch data, the reticle configuration of Scanner flight 1, and the right ascension and declination of cataloged stars were used to generate simulated star transit-time data. The simulated transit times plus expected errors and the right ascension and declination values of the transited stars were processed by the parameter identification program in the same manner as flight data. In addition, the a priori estimates used in this processing were identical to those used for flight data processing. The values of the nine parameters determined by the parameter identification program along with the known values of β_V, β_S, γ_V, and γ_S were used to generate time histories of the pointing directions of the spacecraft principal spin and the star-mapper optical axes. The variation of error in these pointing directions as a function of several parameters was investigated and is presented

in the following sections. These parameters include the length of time covered by a least-squares data fit in terms of fractional parts of a precession cycle, number of stars per spin period used in the data fit, and angular separation of stars within a spin period.

Generation of error time histories.- Since the information provided by the star mapper was transit times of observed stars, the basic errors in the system were inaccuracies in the detection of transit times for the vertical and slanted slit planes. The two sources of error which contributed to these transit time errors were the inaccuracies in time detection of a star transit across the slit planes and resolution of system clock time. As previously discussed, these two error contributions were $\pm T/2$ microseconds and ± 5 microseconds. The total time error was conservatively assumed to be the sum of the two errors or $\pm\frac{T}{2} + 5$ microseconds. This total time error was assumed to have a uniform probability density function and therefore a standard deviation of approximately 19 microseconds for the nominal value of T being approximately 56 microseconds. In the simulation studies, errors having a standard deviation of approximately this value were added to the transit-time data, by selecting, with equal probability, error values of 26, 0, or -26 microseconds.

Different sequences of random time errors were added to each selected sample size of the simulated data. Thus, for each sample size of star data, a run through the least-squares program was necessary for each noise sequence to determine the resulting estimates of the original nine parameters specifying vehicle dynamics. Each set of nine parameters was then fed into a time-history generator, that is, the vehicle dynamic equations written as a function of time. Beginning at time zero, and for equal intervals of time, a time history of attitude data in celestial coordinates (right ascension and declination) for the vehicle symmetry axis $\hat{k}_6$ and the star-mapper optical axis $\hat{i}_8$ was calculated for each set of nine unknowns. Each of these time histories was computed for the length of time covered by the selected sample size of simulated data used in the least-squares program. This computation provided time-history records of attitude both at the times of star sightings and during the periods of time between star sightings. The attitude data representing times between star sightings provide a measure of the interpolation capability of the attitude-determination procedure. Each time history associated with a transit-time noise sequence was compared with a reference time history generated by use of the original nine parameters used in the simulation program. This comparison resulted in an ensemble consisting of as many error time histories in right ascension and declination for the $\hat{k}_6$ and $\hat{i}_8$ axes as the number of noise sequences used in the generation of pointing-direction time histories.

Pointing-direction errors.- Standard-deviation calculations of the errors in right ascension $\sigma_\alpha(t_\nu)$ and declination $\sigma_\delta(t_\nu)$ for each of these axes were made across the ensemble at specific instants of time t_ν. For example, a right-ascension standard-deviation calculation at a specific instant of time is designated as $\sigma_\alpha(t_\nu)_6$ and $\sigma_\alpha(t_\nu)_8$

for the vehicle principal axis and the star-mapper optical axis, respectively. The expected standard-deviation error in pointing direction $\sigma_a(t_\nu)$ of the $\hat{k}_6$ or $\hat{i}_8$ axis was assumed to be the root sum square of the standard deviation of the errors in right ascension and declination of each of these axes. The maximum value of this root sum square value calculation is defined in this report as $\sigma_a(t_\nu)_{max}$ and was determined by computing the value of $\sigma_a(t_\nu)$ at each t_ν and then selecting the maximum value of $\sigma_a(t_\nu)$. Spacing of the time points t_ν was examined for 0.25 second and 0.01 second, negligible differences being noted in the standard-deviation calculations. The root-mean-square value of the pointing-direction error was calculated for the time duration of several error time histories. It is interesting to note that the results of these calculations agreed with standard-deviation calculations made on an ensemble basis to within approximately 15 percent. The use of ten sequences of data for these calculations and application of the chi-squared test resulted in a 99-percent confidence that the true value of $\sigma_a(t_\nu)_{max}$ would lie in the range

$$0.618\sigma_a(t_\nu)_{max} \leqq \text{true } \sigma_a(t_\nu)_{max} \leqq 2.278\sigma_a(t_\nu)_{max}$$

Summary of pointing-direction-error analysis.- The values of the nine parameters used in the generation of the simulation data were

$$\theta = 0.310758^o$$

$$\psi_o = 51.081051^o$$

$$\dot{\psi} = 287.844975^o/\text{sec}$$

$$\phi_o = 316.572701^o$$

$$\dot{\phi} = 19.137575^o/\text{sec}$$

$$\Phi = 76.462935^o$$

$$\Theta = 54.126671^o$$

$$\epsilon_1 = 0.064170^o$$

$$\epsilon_2 = 0.031017^o$$

The vehicle inertia values were assumed to be

$$I_1 = I_2 = 129.92 \text{ slug-ft}^2 \quad (176.15 \text{ kg-m}^2)$$

$$I_3 = 8.27 \text{ slug-ft}^2 \quad (11.2 \text{ kg-m}^2)$$

A partial listing of the simulated star transit data is

SIMULATION DATA LIST

Star	Transit time, sec		Visual magnitude	Boss catalog number
	Vertical slit	Slanted slit		
154	3.908927	3.912402	3.000	19607
172	3.966026	3.971817	2.310	20947
177	3.979605	3.996827	2.000	21491
219	4.183629	4.193429	2.940	25180
221	4.196009	4.211718	3.300	25661
225	4.211204	4.229113	2.710	26161
239	4.293068	4.304024	3.210	28682
23	4.503505	4.505614	3.420	3584
43	4.652463	4.653949	2.920	6274
48	4.690902	4.702167	1.700	6668

The star number is the order of occurrence for the star in the Boss catalog.

Information from this listing which is used by the least-squares program includes the star index number and the transit times for the star across the two slits. The star number was used for a storage index number of the right ascension and declination values of the particular star transited.

The accuracy of the attitude-determination procedure was determined by calculating $\sigma_a(t_\nu)_{max}$ from data representing multiples of a precession period, number of star sightings per spin period, and angular displacement of stars within a spin period. The results of these calculations showed that star placement within a spin period was a major factor, since with poorly placed stars, for example, all stars in a spin period are placed within half a period, precession information is not well defined. As indicated in figure 13, the accuracy of attitude determination increased as the data-fit period used in the least-squares program increased and as the number of star sightings per spin period increased for the one-precession-cycle case. The one-half precession-cycle case also indicates evidence of this trend. The one-and-one-half precession-cycle case shows no particular trend and the results for this case were interpreted to mean that the errors in the estimates of $\underline{X}$ were in the noise level for any considered number of stars per spin period. Based on the plots of figure 13, the predicted Scanner star mapper accuracy was estimated to have a $\sigma_a(t_\nu)_{max}$ value of approximately 0.004^o since most of the least-squares-data fitting covered flight-data periods of three-fourths of a precession cycle and contained at least 4 to 6 star sightings per spin period. The values of $\sigma_a(t_\nu)_{max}$

obtained in the simulation study gave assurance that the attitude-determination technique would meet the experimental requirement of a σ_a of 0.016^o with a confidence level of 99 percent.

Relation of Transit-Time Errors to Least-Squares Functional Residuals

To evaluate the accuracy of attitude determination resulting from use of the estimates of $\underline{X}$ as computed in the least-squares program, time errors ϵ_{tk} were added to the simulated star transit times t_k. The values of ϵ_{tk} had an equal probability of having values of +26, 0, or -26 microseconds and a standard deviation σ_t of approximately 21 microseconds. Since it is not possible to measure σ_t for flight data, it was necessary that some other parameter be used to estimate the magnitude of transit time errors. The functional residuals of the least-squares solutions resulting from simulated data were examined for this purpose.

The adequacy of any estimate of $\underline{X}$ may be determined by the use of certain assumptions. If $\tilde{\underline{X}}^{(j+1)}$ is assumed to be a good enough estimate to allow the use of $\tilde{\underline{X}}^{(j+1)}$ and true kth transit time t_k^t to satisfy approximately the constraint of equation (25), then

$$J_2 DEH\underline{R} \approx 0 \tag{31}$$

For convenience, let the functional dependence of equation (31) on $\underline{X}$ and t for any star and the $(j + 1)$st estimate be denoted by

$$J_2 DEH\underline{R} = f\left(\tilde{\underline{X}}^{(j+1)}, t_k^t\right) \tag{32}$$

Equation (32) may be approximated by a Taylor's series expansion about the true time t_k^t as

$$f\left(\tilde{\underline{X}}^{(j+1)}, t_k^t\right) \approx f\left(\tilde{\underline{X}}^{(j+1)}, t_k^t - \Delta t_k\right) + \left.\frac{\partial f\left(\tilde{\underline{X}}^{(j+1)}, t\right)}{\partial t}\right]_{t=t_k^t-\Delta t_k} (\Delta t_k) \tag{33}$$

By defining

$$t_k^t - \Delta t_k = t_k \tag{34}$$

as any observed transit time, and by setting $f\left(\tilde{\underline{X}}^{(j+1)}, t_k^t\right)$ equal to zero by use of equation (31), the time error in the observed kth star transit time may be approximated by

$$\Delta t_k \approx \frac{-f\left(\tilde{\underline{X}}^{(j+1)}, t_k\right)}{\left.\frac{\partial f\left(\tilde{\underline{X}}^{(j+1)}, t\right)}{\partial t}\right]_{t=t_k}} \tag{35}$$

The convergence factor M was adjusted until a least-squares iteration resulted in time residual values Δt_k which agreed with ϵ_{tk} to within an accuracy of 5 microseconds. In this study the standard deviation of Δt_k was calculated for each set of k stars used in a least-squares solution. This standard deviation of the time residuals σ_{tr} was found to be approximately 20 microseconds for all cases in the study. For $\sigma_{tr} \approx 20$ microseconds, the accuracy of the computed vehicle-attitude orientation was well within the specified requirements. This parameter σ_{tr} was the factor which was used to assess the adequacy of a least-square solution for flight data. In the case of flight data, the convergence factor M was adjusted until σ_{tr} was near its minimum value. When σ_{tr} was at an acceptable minimum value, a least-squares solution was accepted as an adequate one.

Individual values of Δt_k were also used to assess the adequacy of each least-squares solution using flight data. If one or more values of Δt_k in a set of k data points were inordinately larger than the remaining members of the set, the questionable data points were reexamined. In every case the large values of Δt_k could be attributed to errors in range time counting, incorrectly cataloged right ascension or declination values of the star associated with the particular data point, or false star identification resulting from two or more detectable stars appearing in the star-mapper field of view simultaneously. The errors in range time were relatively easy to locate since a taped time-history record of range time counting was available. The errors in cataloged star data were determined by cross checking several astronomical tables of star listings. The identity of the incorrectly cataloged stars and the procedure for handling multiple stars in the field of view are discussed in the section "Flight Results."

Extrapolation of Attitude Determination

The star-mapper data-processing procedure was further studied to determine the feasibility of predicting or extrapolating in time the pointing directions of the $\hat{i}_8$ and $\hat{k}_6$ axes based on the results of the least-squares program. In this study the extrapolation period covered a period of time approximately 1 precession cycle after the period of time used in the least-square solution of the nine parameters defining the vehicle equations of motion. The ability to predict or extrapolate attitude information was limited by transit time errors and the convergence criterion used in the least-squares program. The two principal members of the set of estimated nine parameters which affected the ability to predict attitude were $\dot{\phi}$ and $\dot{\psi}$. The region of extrapolation was also governed by the allowable magnitude of $\sigma_a(t_\nu)$. Inconclusive results were obtained in this study and extrapolation for more than a fractional part of a precession cycle was not possible. It was therefore decided not to attempt attitude extrapolation by use of Scanner flight data.

FLIGHT RESULTS

The star mapper was flown on two suborbital flights of the Scanner vehicles to provide data necessary for determining celestial attitude of these vehicles. On both flights, a cold-gas-reaction jet-control system was used to erect the vehicle to within $\pm 2^{\circ}$ of the local vertical at four definite times during the flight in order to maximize the data gathering of the primary-horizon-definition experiment. During the intervals between these erection times, the controls were turned off and the spin-stabilized vehicle was assumed to be free of external and control torques. Star mapper data for each of the two Scanner flights consisted of four such data periods, each of which was approximately $2\frac{1}{2}$ minutes in duration. Had the vehicle actually been a symmetrical, rigid, torque-free, spinning body, the vehicle's motion for an entire data period could have been represented by a single set of nine vehicle motion parameters. Under this assumption the single set of nine vehicle motion parameters could have been determined by performing a least-squares fitting of all the star transit times in an entire data period. Preliminary evaluation of the results of the attitude determination procedure for both flights indicated that some undefined source produced small disturbing torques during the data periods.

Desired accuracies in the determination of vehicle attitude were obtained with the assumed model by reducing the time periods covered by a least-squares solution to approximately three-fourths of a precession cycle in order to minimize the effects of these torques and possible vehicle asymmetries. For example, the second data period of Scanner flight 1 was divided into 12 time intervals and 12 sets of nine vehicle motion parameters were used to define the vehicle's motion during that data period as shown in table IV. The discrepancy between the model assumed for the motion of the vehicle in the parameter-identification program described earlier and the actual vehicle motions may be seen by observing the total angular spin rate ω, which is defined by

$$\omega = \dot{\psi} + \dot{\phi} \cos \theta$$

For a symmetrical, rigid, spinning, torque-free body, this angular spin rate should remain constant. Spin rate determined by succeeding solutions of approximately three-fourths of a precession cycle over an entire data period was slowly but constantly increasing. This constantly increasing spin rate was characteristic of all four data periods of both Scanner flights. The spin rate obtained for the second data period of flight 1 is shown in figure 14. The increase of ω over the time period of the data period of figure 14 was 0.04 percent. This percentage of increase for ω was approximately the same for all data periods of both flights. No attempt was made to determine the source of this variation in the assumed model. A possible source of the small disturbing torques could have been incomplete closure of the control valves in the reaction-jet control system during the data period.

The number of stars per spin period sighted by the star mapper during each data period varied from 3 to 14. The listing of identified stars sighted by the star mapper technique during the Scanner flight 1 is shown in table V. Ambiguities in associating raw data with vertical or slanted slit transits and in star identification were encountered when two or more stars with small angular separations were present in the field of view of the star mapper. Such problems usually resulted in unusable data from one or both stars, in which case the questionable stars were eliminated from the star identification list. As a result, the number of stars actually used for attitude determination of the Scanner vehicles, shown in table VI, was considerably smaller than the number identified.

Preliminary data results revealed that several stars consistently exhibited large time residuals. Subsequent checking traced the cause of these high residuals to errors in the updated star positions based on values listed in the Boss catalog. The positions of these stars (δ Orionis, η Ursae Majoris, and α Piscis Austrini) were cross checked with positions taken from the apparent place tables (ref. 8) and updated to the nearest 0.1 day of the flight. Discrepancies of the order of 0.01° in the star positions taken from the Boss catalog and updated to the nearest 0.1 day of flight were found. When the stars' positions determined from the apparent place tables were used for these stars, the time residuals for these stars dropped to acceptable limits.

An analysis of all solutions of the nine vehicle-motion parameters determined from flight data showed a time residual σ_{tr} of approximately 30 microseconds. In the simulation study described in an earlier section, star-transit-time errors having a standard deviation of approximately 21 microseconds were added to the simulated star transit data. These time errors resulted in a standard deviation of the time residuals σ_{tr} of approximately 20 microseconds when data were fitted over an interval of 0.5 to 1.50 precession cycles. The corresponding maximum error in the pointing direction σ_a was found to be approximately 0.004°. It can be shown analytically that there is a linear relationship between σ_a and σ_t. Since it has been shown that σ_t and σ_{tr} have very close agreement, it can be said that there is approximately a linear relationship between σ_a and σ_{tr}. Therefore, the expected accuracy in pointing direction determined from flight data is approximately 0.006°. Although the time residuals were somewhat larger than the transit time errors used in the simulation study, the accuracy of the data still remained within acceptable limits for the flight experiment.

To illustrate the use of the nine vehicle-motion parameters, a set of these parameters was selected from the second data period of Scanner flight 1 and was used to generate time histories of the star-mapper optical axis $\hat{i}_8$ and the vehicle principal spin axis $\hat{k}_6$. The results of these computations are shown in figures 15 and 16 in which the pointing directions of these two axes are plotted in terms of declination and right ascension for selected time periods. Figure 15 represents the pointing direction of the optical axis during one spin period and figure 16 represents the pointing direction of the vehicle

principal spin axis during a precession cycle. Figure 17 represents the pointing direction of the $\hat{k}_8$ axis during a precession cycle. The vehicle motion parameters used to generate this plot were the same ones as used for figure 16. Figure 17 illustrates the effects of the misalinement angles, ϵ_1 and ϵ_2. The complete listing of all the sets of nine parameters for each data period and for both flights was used in a similar manner to generate time histories for the $\hat{i}_8$ axis. These results along with the preflight measured angular relationship between the star-mapper $\hat{i}_8$ axis and each radiometer optical axis were used to determine the time history of each radiometer optical axis in celestial coordinates.

POSSIBLE EXTENSIONS OF THE METHOD OF ATTITUDE DETERMINATION

If the reported attitude-determination technique is used in future space flights, several areas of the data-processing procedures should be modified to facilitate data handling. The extent of the modifications depends on the particular application. However, in any future application, it would be desirable to eliminate, as much as possible, manual data handling, particularly in the areas of pairing of apparent star observation times and star identification. Increased automation in these areas may require that the entire data-processing procedure be a closed-loop operation. For application to an orbiting spacecraft, a more exact model of the dynamical equations of motion would be required. This model should include the effects of vehicle asymmetries and at least the most significant external disturbance torques for the spacecraft under consideration. Methods other than the reported least-squares method used for the solution of the undetermined parameters in the equations of motion should be investigated. In particular, sequential updating methods such as the Kalman filter should be studied for application to long-life orbiting spacecraft.

A least-squares solution may be improved by using the time residuals to correct for errors in star transit times. Use of these time residuals to correct star-transit-time data is expected to result in improved least-squares solutions and therefore improved attitude-determination accuracy provided that the model of the vehicle equations of motion is well known. If greater attitude determination accuracies were required for the Scanner flights, this method could be investigated for possible improvement of the achieved accuracies. The value of this method would first need to be evaluated for the cases in which the true vehicle dynamics and the assumed model dynamics differed.

If the transit time errors are truly random, the time residuals will exhibit no preferred periodicities. In the case of the Scanner flights, periodicities which agreed with the periodicities of the radiometer scan mirrors were observed in the time residuals.

This result was expected since preflight analysis of the effects of motion of the radiometer scan mirrors indicated that the vehicle moments of inertia would vary with a period equal to the period of the scanning mirrors. The maximum predicted change in the moments of inertia based on the mirror scan motion was 0.017 percent. Simulation studies indicated that asymmetries of this amount would produce negligible error in attitude determination when a symmetrical model was assumed. The important point is that the time residuals of the Scanner flight contained periodicities which were directly attributable to ignored but known sources which contributed to the vehicle dynamics. Thus the time residuals might be used to reveal periodicities attributable to unknown sources. This information could then be used to define a more exact dynamical model.

CONCLUDING REMARKS

An attitude-determination technique using star-transit information has been successfully demonstrated with an estimated accuracy greater than 0.01° during suborbital flights of the spin-stabilized Scanner spacecraft. Identification of the sensed stars was made on the basis of their angular separations in the celestial sphere as determined from their transit times. Information consisting of the cataloged positions of these identified stars and their measured transit times was fitted in a least-squares method to a set of equations representing an assumed dynamic model of the spacecraft attitude. The dynamical model was developed on the assumptions that the vehicle was spin-stabilized, symmetrical, and free of external torques. The least-squares fitting of star position and transit time data resulted in definition of sets of parameters of the assumed dynamical model. The equations of the model and the sets of parameters were then used to generate time histories of selected reference frames associated with the model. In particular, time histories were determined for pointing directions of the vehicle principal spin axis and the star-mapper optical axis. Accuracy of the solution of the attitude determination problem was based on the pointing-direction accuracy of the star-mapper optical axis which was the only axis that could be related to the radiometer lines of sight.

Estimated accuracies of the pointing-direction determination of the star-mapper optical axis from flight results agreed favorably with predicted results. The achieved accuracies were considered to surpass the results obtained from other attempts to measure or determine celestial attitude of a spin-stabilized spacecraft.

Differences between the predicted results and actual results were evidenced by greater transit-time residuals in the flight data. These larger time residuals may be attributed to either an increase of noise or to an inexact model of the assumed vehicle dynamics. The latter reason is considered to be the most probable since it was observed that total spin rate steadily increased as a function of flight time. A source of this

problem might have been incomplete closure of the control valve in the reaction-jet control system.

Langley Research Center,
National Aeronautics and Space Administration,
Langley Station, Hampton, Va., May 6, 1968,
715-02-00-01-23.

APPENDIX A

PREFLIGHT MEASUREMENTS OF THE RETICLE AND DESCRIPTION OF THE DETERMINATION OF THE SLIT PARAMETER ANGLES

The angular relationship between the slit plane, defined by the $\hat{i}_{10} - \hat{k}_{10}$ plane, and the $\hat{i}_{10} - \hat{k}_8$ plane of figure 7 is defined as the angle β. The actual experimental measurements of the reticle configuration have been described in reference 3, and no attempt is made to redescribe these measurements. However, since an understanding of the geometry of this measurement is essential to any discussion of the method of determining the angle β, a summary of the method described in reference 3 is discussed here.

A collimator beam was used as a light source and the star mapper was mounted on a table which could be moved in azimuth and elevation. The table could be locked in elevation and moved in the azimuth direction. As nearly as possible, the vertical slit group was fixed so that it was perpendicular to the azimuthal plane of the table. The nonverticalness of the vertical slits to the table azimuthal plane is accounted for in the computation of β. The star mapper and table were positioned such that the collimator beam was at the center of the alinement point. The alinement point defines 0^o in the elevation and 0^o in the azimuthal plane of the table.

With the table locked at an elevation of 0^o, the table was rotated in the azimuthal plane until the collimator beam was coincident with the leading edge of the vertical slit group at a point defined as V_o. The azimuthal angle of this rotation, defined as ρ_{V_o}, was recorded.

The table was then returned to the alinement point $(0^o,0^o)$ and rotated in the opposite direction until the collimator beam was coincident with the leading edge of the slanted slit as S_o and the azimuthal separation between the alinement point and the leading edge of the slanted slit, defined as ρ_{S_o}, was recorded also. In figure 18 ON defines the axis about which azimuth was measured and P is the alinement point which defines 0^o elevation and 0^o azimuth.

When the table was returned to the $(0^o,0^o)$ position and elevated to an angle ξ, the elevation axis was then positioned at P_ξ with $\widehat{NP}_\xi$ defined by an arc of length $(90^o - \xi)$ as shown in figure 18. The azimuthal angle $\rho_{S\xi}$ was measured by the rotation about ON from P_ξ to S_ξ.

The spherical angle $S_\xi NS_o$ is denoted by λ where

$$\lambda = \rho_{S\xi} - \rho_{S_o} \tag{A1}$$

APPENDIX A

The angle β_1 defines the angle of nonverticalness of the slanted slit group with the azimuthal plane of the table.

By the law of sines for spherical triangles,

$$\sin \beta_1 = \frac{\cos \xi \sin \lambda}{\sin \widehat{S_o S_\xi}} \tag{A2}$$

Since the arc $\widehat{S_o N}$ equals 90^o, the law of cosines reduces to

$$\cos \beta_1 = \frac{\sin \xi}{\sin \widehat{S_\xi S_o}} \tag{A3}$$

Dividing equation (A2) by equation (A3) reduces to the form

$$\tan \beta_1 = \frac{\sin \lambda}{\tan \xi} = \frac{\sin\left(\rho_{S\xi} - \rho_{So}\right)}{\tan \xi} \tag{A4}$$

This same process was repeated for the vertical slit group to obtain a corresponding angle β_2 between its leading edge and the plane perpendicular to the azimuthal plane of the table at point V_o on the leading edge of the vertical slit group. The resulting equation, similar to that for β_1, defines β_2

$$\tan \beta_2 = \frac{\sin\left(\rho_{V\xi} - \rho_{Vo}\right)}{\tan \xi} \tag{A5}$$

The angle between the slanted slit plane and the $\hat{i}_{10} - \hat{k}_8$ plane of figure 7 is defined by the angle β_S as

$$\beta_S = \beta_1 + \beta_2 \tag{A6}$$

and the angle between the vertical slit plane and the $\hat{i}_{10} - \hat{k}_8$ plane is defined as

$$\beta_V = 0 \tag{A7}$$

In each case the slit plane is defined as the $\hat{i}_{10} - \hat{k}_{10}$ plane of figure 7. Preflight measurements were also made to determine the azimuthal separation between the leading and trailing edges of the vertical and slanted slit groups.

The azimuthal angular relationship of the vertical slit plane to the optical axis is defined as

$$\gamma_V = \rho_{Vo} - 9.25\mu \tag{A8}$$

The azimuthal angular relationship between the slanted slit plane and the optical axis is defined as

$$\gamma_S = \rho_{So} - 9.25\mu \tag{A9}$$

APPENDIX A

The preflight measurements indicated a different value of μ for the vertical and slanted slit groups. The measured values of μ for the vertical and slanted slit groups were used in equations (A8) and (A9), respectively.

APPENDIX B

IDENTIFICATION OF STAR TRIPLETS

Recall from figure 4 that the star-mapper data at the input to the star-identification program were in the form of star-transit-time pairs where each transit-time pair resulted from observation of a single star. This time listing was grouped in triplets of transit-time pairs for each vehicle spin period which was obtained from ω_{est}. This grouping is illustrated in the following example sketch:

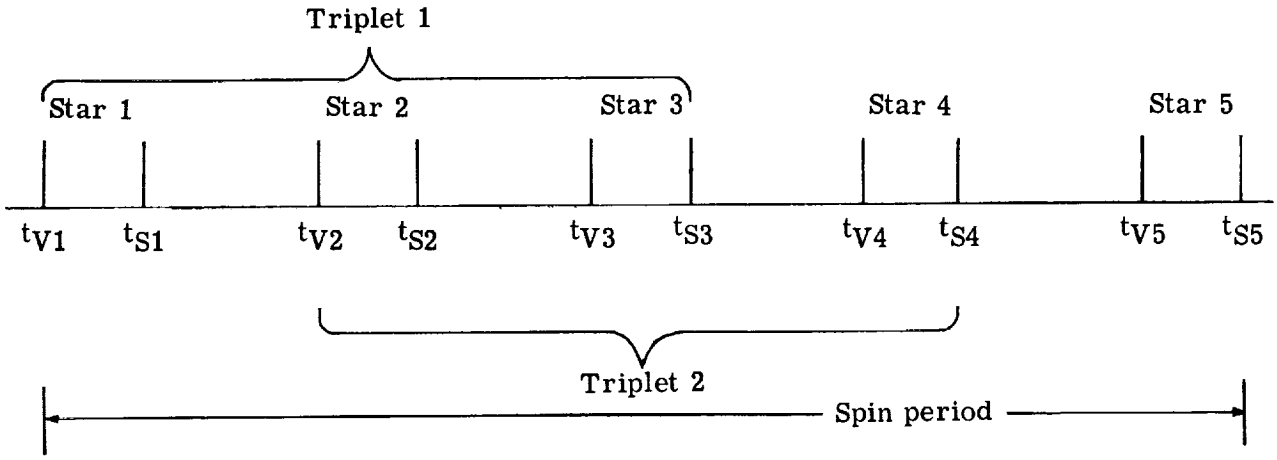

The first triplet is composed of transit-time pairs 1, 2, and 3 and the second triplet is composed of star-transit-time pairs 2, 3, and 4. This grouping into triplets was continued until all transit-time pairs in a spin period were exhausted.

The angular separation of each pair of stars in a triplet was determined by equation (11). These angular separations were used to obtain prime candidates for the observed star pairs from the reference list of stars. As many sets of prime candidates were selected for stars 1 and 2, then 1 and 3, and finally 2 and 3 as could satisfy equation (12). If this is done properly, at least one of the prime candidates for star 1 of (1,2) and star 1 of (1,3) should be the same. This procedure was repeated to identify star 3 of (1,3) and (2,3), and star 2 of (1,2) and (2,3).

This procedure is illustrated by the following example: Given a computed angular separation of two observed stars, the listing of angular separations of all pairs of stars in the reference list was searched for angular separations meeting the condition of equation (12). Each pair of observed stars was associated with a sublisting of prime candidates taken from the reference star list. After this procedure was completed for stars (1,2), (2,3), and (3,1), the following sublists of prime candidates were available:

APPENDIX B

Prime candidate star pairs from reference list for observed star pairs –		
1,2	2,3	3,1
1,5	5,6	9,1
[7,9]	[9,29]	9,4
7,17	14,17	[29,7]
18,22	22,29	30,18
41,42	33,36	

The star numbers denoting candidate stars merely refer to the index numbers chosen for the reference list of stars and should not be confused with Boss catalog numbers. Simultaneous comparison of the three lists of prime candidates should yield one triplet of reference stars for the triplet of observed stars 1, 2, and 3. In the example, it is apparent that the only triplet of reference stars which has common stars in each of the three lists of candidates star pairs is 7, 9, and 29. This comparison results in a tentative identification of observed stars 1, 2, and 3 as reference stars 7, 9, and 29, respectively.

Sometimes a triplet of observed stars was tentatively identifiable by more than one triplet of reference stars. The ambiguity was overcome by using the identified stars of each possible triplet and the associated six transit times in a least-squares program to solve for the reduced set of parameters $\phi + \psi$, Θ, and Φ. All triplets were rejected when values of Θ and Φ disagreed by more than $\pm 10^{o}$ from the launch-data estimates of these two angles. The triplet which produced the smallest functional residual in the least-squares program was selected as the identified triplet out of all the remaining triplet candidates.

Once a triplet was tentatively identified, the index numbers of the identified reference stars were stored in a sample table as follows:

Sequence of stars in a triplet	Triplet number						
	1	2	3	4	5	6	7
1	60	0	0	0	0	0	0
2	0	1	0	0	0	0	0
3	0	0	16	0	0	0	0

APPENDIX B

Identification of the second triplet stars ideally reproduces the index numbers 1 and 16, since the next triplet is obtained by dropping the first star and adding a new one at the end. In the example, the added star is assumed to be index number 38 which yields

Sequence of stars in a triplet	Triplet number						
	1	2	3	4	5	6	7
1	60	1	0	0	0	0	0
2	0	1	16	0	0	0	0
3	0	0	16	38	0	0	0

If the program was unable to identify the stars in a triplet, a negative number (-1, -2, or -3) was stored in the table in place of a reference star index number, as indicated in the following list representing the identification of all stars in a complete spin period:

Sequence of stars in a triplet	Triplet number						
	1	2	3	4	5	6	7
1	60	1	-1	38	57	0	0
2	60	1	16	-2	57	60	0
3	60	1	16	38	-3	60	1

The final step in the identification process was to examine the reference star index numbers in all but the last two columns of the table of identified stars for identical index numbers. If two or more index numbers in each column were identical, then positive identification was assumed for the reference star associated with that index number. If no two index numbers in a column were alike, identification was not made. Identification of the first and second star in a spin period required that the first two transit-time pairs be updated by a spin period, the star pair representing these modified transit times be repeated at the end of the list, the second and third entries of the next to last column be copied into the first column, and the third entry of the last column be copied in the second column.

The authors wish to acknowledge the contribution of Bruce Vannelli of Control Data Corporation who, in the course of writing a digital computer program for star identification, developed the logic used in the identification of stars.

APPENDIX C

LEAST-SQUARES FORMULATION FOR SMALL CONE ANGLES

Equation (25) may be expanded in a Taylor series expansion as

$$0 \approx J_2 DEH\underline{R} + F_2\left(\underline{\tilde{X}}\right)\Delta\underline{X} \tag{C1}$$

with terms higher than the first variational terms assumed to be negligible. The matrix $F_2\left(\underline{\tilde{X}}\right)$ is defined as

$$F_2\left(\underline{\tilde{X}}\right) = \left(\frac{\partial}{\partial X_1}, \frac{\partial}{\partial X_2}, \frac{\partial}{\partial X_3}, \frac{\partial}{\partial X_4}, \frac{\partial}{\partial X_5}, \frac{\partial}{\partial X_6}, \frac{\partial}{\partial X_7}, \frac{\partial}{\partial X_8}, \frac{\partial}{\partial X_9}\right) J_2 DEH\underline{R} \tag{C2}$$

where the partial derivative operators are defined as

$$\begin{pmatrix} \frac{\partial}{\partial X_1} \\ \frac{\partial}{\partial X_2} \\ \frac{\partial}{\partial X_3} \\ \frac{\partial}{\partial X_4} \\ \frac{\partial}{\partial X_5} \\ \frac{\partial}{\partial X_6} \\ \frac{\partial}{\partial X_7} \\ \frac{\partial}{\partial X_8} \\ \frac{\partial}{\partial X_9} \end{pmatrix} = \begin{pmatrix} \frac{\partial}{\partial \theta} \\ \frac{\partial}{\partial \psi_o} \\ \frac{\partial}{\partial \dot{\psi}} \\ \frac{\partial}{\partial \phi_o} \\ \frac{\partial}{\partial \dot{\phi}} \\ \frac{\partial}{\partial \Phi} \\ \frac{\partial}{\partial \Theta} \\ \frac{\partial}{\partial \epsilon_1} \\ \frac{\partial}{\partial \epsilon_2} \end{pmatrix} \tag{C3}$$

Equation (C1) is a general expression for any star transit time where the matrix E is the only matrix dependent upon θ. The problem arising from a zero or small θ may be illustrated by examination of this matrix E. The matrix E may be written as

$$E(\phi,\theta,\psi) = A(\phi + \psi) + \sin\theta B(\phi,\psi) + (1 - \cos\theta)C(\phi,\psi) \tag{C4}$$

where

$$A = \begin{bmatrix} \cos(\psi + \phi) & \sin(\psi + \phi) & 0 \\ -\sin(\psi + \phi) & \cos(\psi + \phi) & 0 \\ 0 & 0 & 1 \end{bmatrix}$$

$$B = \begin{bmatrix} 0 & 0 & \sin\psi \\ 0 & 0 & \cos\psi \\ \sin\phi & -\cos\phi & 0 \end{bmatrix}$$

$$C = \begin{bmatrix} \sin\phi\sin\psi & -\cos\phi\sin\psi & 0 \\ \sin\phi\cos\psi & -\cos\phi\cos\psi & 0 \\ 0 & 0 & -1 \end{bmatrix}$$

From equation (C4) it is clear that for zero θ,

$$E(\phi,0,\psi) = A(\phi + \psi)$$

and for θ small, for which $\sin\theta$ and $(1 - \cos\theta)$ are small,

$$\frac{\partial E}{\partial \psi_o} \approx \frac{\partial E}{\partial \phi_o}$$

and

$$\frac{\partial E}{\partial \dot{\psi}} \approx \frac{\partial E}{\partial \dot{\phi}} \approx t\,\frac{\partial E}{\partial \psi_o} \approx t\,\frac{\partial E}{\partial \phi_o}$$

The matrix multiplier of $\Delta\underline{X}$ in equation (C1) therefore has two pairs of columns which are nearly equal. Since the matrix $\left[F_2\left(\underline{\tilde{X}}^{(j)}\right)_k\right]^T\left[F_2\left(\underline{\tilde{X}}^{(j)}\right)_k\right]$ of equation (26) is determined by use of this matrix multiplier, the $\left[F_2\left(\underline{\tilde{X}}^{(j)}\right)_k\right]^T\left[F_2\left(\underline{\tilde{X}}^{(j)}\right)_k\right]$ matrix is clearly singular for zero θ or nearly singular for very small θ. The physical reason for this problem is that for small θ, the angles ϕ_o and ψ_o are poorly defined individually and only their sum is well defined. Similarly, only the sum of the rates $\dot{\phi}$ and $\dot{\psi}$ are well defined for small θ.

The approach to the singularity problem arising from small cone angles was to find a new set of parameters $\underline{Y}$ rather than $\underline{X}$, solve a modified least-squares problem for $\Delta\underline{Y}$, and then perform a transformation from the $\Delta\underline{Y}$ vector to the $\Delta\underline{X}$ vector. During

the course of writing a digital computer program for the least-squares equations, Mr. Charles B. Grosch of Control Data Corporation suggested the new ΔY vector:

$$\Delta\underline{Y} = \begin{pmatrix} \Delta\theta \\ \Delta\phi_o + \Delta\psi_o \\ \Delta\dot{\phi} + \Delta\dot{\psi} \\ \Delta\Phi \\ \Delta\Theta \\ 2\Delta\phi_o \sin\frac{\theta}{2} \\ 2\Delta\dot{\phi} \sin\frac{\theta}{2} \\ \Delta\epsilon_1 \\ \Delta\epsilon_2 \end{pmatrix} \tag{C5}$$

which was successfully applied to the singularity problem. Substituting equation (C5) into equation (C1) results in

$$0 \approx J_2 DEH\underline{R} + V\Delta\underline{Y} \tag{C6}$$

where the matrix V^T is defined as

$$V^T = \begin{pmatrix} J_2 D(\cos\theta B + \sin\theta C)H\underline{R} \\ J_2 D\left(A_\psi + \sin\theta\, B_\psi + (1 - \cos\theta)C_\psi\right)H\underline{R} \\ tJ_2 D\left(A_\psi + \sin\theta\, B_\psi + (1 - \cos\theta)C_\psi\right)H\underline{R} \\ J_2 DEH_\Phi\underline{R} \\ J_2 DEH_\Theta\underline{R} \\ J_2 D\left(\cos\frac{\theta}{2}(B_\phi - B_\psi) + \sin\frac{\theta}{2}(C_\phi - C_\psi)\right)H\underline{R} \\ tJ_2 D\left(\cos\frac{\theta}{2}(B_\phi - B_\psi) + \sin\frac{\theta}{2}(C_\phi - C_\psi)\right)H\underline{R} \\ J_2 D_{\epsilon 1} EH\underline{R} \\ J_2 D_{\epsilon 2} EH\underline{R} \end{pmatrix} \tag{C7}$$

The subscripts of equation (C7) denote partial differentiation with respect to the particular subscripted parameter. Each star transit time then produces an equation of the form

given by equation (C6) and the system of resulting equations does not possess a singularity for small θ. After a solution is made for ΔY by using the least-squares approach described previously, the correction vector $\Delta\underline{X}$ is found by

$$\Delta\underline{X} = \begin{pmatrix} \Delta\theta \\ \Delta\psi_o \\ \Delta\dot{\psi} \\ \Delta\phi_o \\ \Delta\dot{\phi} \\ \Delta\Phi \\ \Delta\Theta \\ \Delta\epsilon_1 \\ \Delta\epsilon_2 \end{pmatrix} = \begin{pmatrix} \Delta y_1 \\ \dfrac{\Delta y_2 - \Delta y_6}{2 \sin \theta/2} \\ \dfrac{\Delta y_3 - \Delta y_7}{2 \sin \theta/2} \\ \dfrac{\Delta y_6}{2 \sin \theta/2} \\ \dfrac{\Delta y_7}{2 \sin \theta/2} \\ \Delta y_4 \\ \Delta y_5 \\ \Delta y_8 \\ \Delta y_9 \end{pmatrix} \tag{C8}$$

The basis for convergence in the least-squares solution is still the condition that $\Delta\underline{X}^{(j)} \leq M$ as discussed earlier.

REFERENCES

1. Dodgen, J. A.: McKee, T. B.; and Jalink, A.: NASA-LRC Program To Define Experimentally the Earth's IR Horizon. NASA paper presented at the Symposium on Infrared Horizon Sensors for Spacecraft Guidance and Control (El Segundo, Calif.), Mar. 14-15, 1967.

2. Garner, H. D.; and Reid, H. J. E., Jr.: Simulator Studies of Simple Attitude Control for Spin-Stabilized Vehicles. NASA TN D-1395, 1962.

3. Walsh, T. M.; Dixon, William C., Jr.; Hinton, Dwayne E.; and Holland, James A.: A Celestial Attitude Measurement Instrument for Project Scanner. NASA TN D-4742, 1968.

4. Walsh, T. M.; and Kenimer, Robert L.: Analysis of a Star-Field Mapping Technique for Use in Determining the Attitude of a Spin-Stabilized Spacecraft. NASA TN D-4637, 1968.

5. Slater, John C.; and Frank, Nathaniel H.: Mechanics. McGraw-Hill Book Co., Inc., 1947.

6. Boss, Benjamin: General Catalogue of 33 342 Stars for the Epoch 1950. Publ. No. 468, Vols. II-V, Carnegie Inst. of Washington, 1937.

7. Anon.: Explanatory Supplement to the Astronomical Ephemeris and the American Ephemeris and Nautical Almanac. H. M. Nautical Almanac Office, 1961.

8. Anon.: Apparent Places of Fundamental Stars, 1966. Astron. Rechen-Inst., (Heidelberg), 1964.

TABLE I.- THE SEQUENCE OF ROTATIONS AND THE TRANSFORMATION MATRICES FOR THE TEN BASIC REFERENCE FRAMES USED TO DETERMINE SPACECRAFT ATTITUDE

$\begin{pmatrix} \hat{i}_1 \\ \hat{j}_1 \\ \hat{k}_1 \end{pmatrix} = (\Phi) \begin{pmatrix} \hat{i}_2 \\ \hat{j}_2 \\ \hat{k}_2 \end{pmatrix}$	$(\Phi) = \begin{pmatrix} \cos\Phi & -\sin\Phi & 0 \\ \sin\Phi & \cos\Phi & 0 \\ 0 & 0 & 1 \end{pmatrix}$
$\begin{pmatrix} \hat{i}_2 \\ \hat{j}_2 \\ \hat{k}_2 \end{pmatrix} = (\Theta) \begin{pmatrix} \hat{i}_3 \\ \hat{j}_3 \\ \hat{k}_3 \end{pmatrix}$	$(\Theta) = \begin{pmatrix} 1 & 0 & 0 \\ 0 & \cos\Theta & -\sin\Theta \\ 0 & \sin\Theta & \cos\Theta \end{pmatrix}$
$\begin{pmatrix} \hat{i}_3 \\ \hat{j}_3 \\ \hat{k}_3 \end{pmatrix} = (\phi) \begin{pmatrix} \hat{i}_4 \\ \hat{j}_4 \\ \hat{k}_4 \end{pmatrix}$	$(\phi) = \begin{pmatrix} \cos\phi & -\sin\phi & 0 \\ \sin\phi & \cos\phi & 0 \\ 0 & 0 & 1 \end{pmatrix}$
$\begin{pmatrix} \hat{i}_4 \\ \hat{j}_4 \\ \hat{k}_4 \end{pmatrix} = (\theta) \begin{pmatrix} \hat{i}_5 \\ \hat{j}_5 \\ \hat{k}_5 \end{pmatrix}$	$(\theta) = \begin{pmatrix} 1 & 0 & 0 \\ 0 & \cos\theta & -\sin\theta \\ 0 & \sin\theta & \cos\theta \end{pmatrix}$
$\begin{pmatrix} \hat{i}_5 \\ \hat{j}_5 \\ \hat{k}_5 \end{pmatrix} = (\psi) \begin{pmatrix} \hat{i}_6 \\ \hat{j}_6 \\ \hat{k}_6 \end{pmatrix}$	$(\psi) = \begin{pmatrix} \cos\psi & -\sin\psi & 0 \\ \sin\psi & \cos\psi & 0 \\ 0 & 0 & 1 \end{pmatrix}$

TABLE I.- THE SEQUENCE OF ROTATIONS AND THE TRANSFORMATION MATRICES FOR THE TEN BASIC REFERENCE FRAMES USED TO DETERMINE SPACECRAFT ATTITUDE – Concluded

$\begin{pmatrix} \hat{i}_6 \\ \hat{j}_6 \\ \hat{k}_6 \end{pmatrix} = (\epsilon_1) \begin{pmatrix} \hat{i}_7 \\ \hat{j}_7 \\ \hat{k}_7 \end{pmatrix}$	$(\epsilon_1) = \begin{pmatrix} 1 & 0 & 0 \\ 0 & \cos\epsilon_1 & -\sin\epsilon_1 \\ 0 & \sin\epsilon_1 & \cos\epsilon_1 \end{pmatrix}$
$\begin{pmatrix} \hat{i}_7 \\ \hat{j}_7 \\ \hat{k}_7 \end{pmatrix} = (\epsilon_2) \begin{pmatrix} \hat{i}_8 \\ \hat{j}_8 \\ \hat{k}_8 \end{pmatrix}$	$(\epsilon_2) = \begin{pmatrix} \cos\epsilon_2 & 0 & \sin\epsilon_2 \\ 0 & 1 & 0 \\ -\sin\epsilon_2 & 0 & \cos\epsilon_2 \end{pmatrix}$
$\begin{pmatrix} \hat{i}_8 \\ \hat{j}_8 \\ \hat{k}_8 \end{pmatrix} = (\gamma) \begin{pmatrix} \hat{i}_9 \\ \hat{j}_9 \\ \hat{k}_9 \end{pmatrix}$	$(\gamma) = \begin{pmatrix} \cos\gamma & -\sin\gamma & 0 \\ \sin\gamma & \cos\gamma & 0 \\ 0 & 0 & 1 \end{pmatrix}$
$\begin{pmatrix} \hat{i}_9 \\ \hat{j}_9 \\ \hat{k}_9 \end{pmatrix} = (\beta) \begin{pmatrix} \hat{i}_{10} \\ \hat{j}_{10} \\ \hat{k}_{10} \end{pmatrix}$	$(\beta) = \begin{pmatrix} 1 & 0 & 0 \\ 0 & \cos\beta & -\sin\beta \\ 0 & \sin\beta & \cos\beta \end{pmatrix}$

TABLE II.- A PRIORI DATA

	Flight 1	Flight 2
Preflight measurement		
γ_V, deg	2.8659	2.8612
γ_S, deg	-0.1967	-0.2027
β_V, deg	0	0
β_S, deg	43.1513	43.1160
I_1, slug-ft^2	130	135
I_3, slug-ft^2	8.3	8.8
Launch data and flight estimates		
ω_{est}, deg/sec	306.3	239.6
ϵ_1, deg	Unknown	Unknown
ϵ_2, deg	Unknown	Unknown
Φ, deg	75.42	137.5
Θ, deg	50.95	58.5
$^*\dot{\phi}$, deg/sec	19.5	15.52
ϕ_o, deg	Unknown	Unknown
$\dot{\psi}$, deg/sec	286.8	224.08
ψ_o, deg	Unknown	Unknown
θ, deg	Unknown	Unknown

$^*\dot{\phi}$ was estimated with the assumption that $\cos\theta \approx 1$.

TABLE III.- INDIVIDUAL ELEMENTS OF JDEH MATRIX

$$J = \begin{pmatrix} \cos\gamma & \sin\gamma & 0 \\ -\sin\gamma\cos\beta & \cos\gamma\cos\beta & \sin\beta \\ \sin\gamma\sin\beta & -\cos\gamma\sin\beta & \cos\beta \end{pmatrix}$$

$$D = \begin{pmatrix} \cos\epsilon_2 & \sin\epsilon_1\sin\epsilon_2 & -\cos\epsilon_1\sin\epsilon_2 \\ 0 & \cos\epsilon_1 & \sin\epsilon_1 \\ \sin\epsilon_2 & -\sin\epsilon_1\cos\epsilon_2 & \cos\epsilon_1\cos\epsilon_2 \end{pmatrix}$$

$$E = \begin{pmatrix} \cos\psi\cos\phi - \cos\theta\sin\phi\sin\psi & \cos\psi\sin\phi + \cos\theta\cos\phi\sin\psi & \sin\psi\sin\theta \\ -\sin\psi\cos\phi - \cos\theta\sin\phi\cos\psi & -\sin\psi\sin\phi + \cos\theta\cos\phi\cos\psi & \cos\psi\sin\theta \\ \sin\theta\sin\phi & -\sin\theta\cos\phi & \cos\theta \end{pmatrix}$$

$$H = \begin{pmatrix} \cos\Phi & \sin\Phi & 0 \\ -\cos\Theta\sin\Phi & \cos\Theta\cos\Phi & \sin\Theta \\ \sin\Theta\sin\Phi & -\sin\Theta\cos\Phi & \cos\Theta \end{pmatrix}$$

TABLE IV.- VEHICLE MOTION PARAMETERS FOR THE SECOND DATA PERIOD OF SCANNER FLIGHT 1

Time (a)		θ, deg	ψ_o, deg	$\dot{\psi}$, deg/sec	ϕ_o, deg	$\dot{\phi}$, deg/sec	Φ, deg	Θ, deg	ϵ_1, deg	ϵ_2, deg
min	sec									
24	3.23498	-0.315605	257.490643	288.445858	107.284283	18.482840	76.451450	54.130412	0.038607	0.046579
24	14.08154	-.312157	144.903893	287.062817	308.978760	19.882012	76.461610	54.137077	.039603	.045426
24	25.51978	.312637	6.962404	288.093067	357.829037	18.865309	76.456949	54.137756	.027676	.043253
24	33.99485	-.304882	107.741646	287.259624	338.545620	19.710493	76.457376	54.132216	.033905	.044052
24	41.93850	.309047	48.131818	287.881664	316.643620	19.100499	76.454263	54.140100	.040073	.045732
24	52.84173	.310211	307.467949	287.377155	164.405958	19.618340	76.455278	54.144165	.038900	.047986
25	3.49465	.314057	129.948818	287.237286	12.317471	19.770194	76.463597	54.134274	-.000252	.042944
25	15.94554	.308249	107.170229	287.945621	257.622326	19.075793	76.455045	54.128122	.004248	.041465
25	27.93654	.314447	317.269981	287.772449	129.021713	19.257796	76.454346	54.140325	.023696	.042999
25	36.32649	.305107	158.666159	287.572033	287.587963	19.466666	76.453516	54.141089	-.002766	.046548
25	46.69653	.310320	315.331436	287.206608	130.950977	19.842483	76.438763	54.144919	.045223	.049947
25	57.27342	.314742	114.694677	287.473938	339.198837	19.586070	76.445923	54.141324	.029057	.047476

[a]Real time after 0600 UT, August 16, 1966.

TABLE V.- IDENTIFIED STARS OF PROJECT SCANNER FLIGHT 1

Boss catalog number	Name	Bayer name	Apparent visual magnitude	Spectral class
*3584	Acamar	θ Eridani	3.06	A2
6274	Cursa	β Eridani	2.92	A3
6668	Bellatrix	γ Orionis	1.70	B2
6847	Mintaka	δ Orionis	2.48	O9
8208	Tejat Posterior	μ Geminorum	3.19	M3
12407	Talitha	ι Ursae Majoris	3.12	A4
15145	Merak	β Ursae Majoris	2.44	A0
16268	Phekda	γ Ursae Majoris	2.54	A0
17518	Alioth	ϵ Ursae Majoris	1.68	A0
*18133	Mizar	ζ Ursae Majoris	2.17	A2
18643	Alkaid	η Ursae Majoris	1.91	B3
20947	Alphecca	α Corona Borealis	2.31	A0
22193	Kornephoros	β Herculis	2.81	G8
25180	Kaus Borealis	λ Sagittarii	2.94	K0
25661		φ Sagittarii	3.30	B8
25941	Nunki	σ Sagittarii	2.14	B3
*26161	Ascella	ζ Sagittarii	2.71	A2
30942	Alnair	α Gruis	2.16	B5

*Double star.

TABLE VI.- STARS USED TO DETERMINE ATTITUDE OF SCANNER VEHICLES

Boss catalog number	Name	Bayer name	Apparent visual magnitude	Spectral class
Scanner flight 1				
*3584	Acamar	θ Eridani	3.06	A2
6274	Cursa	β Eridani	2.92	A3
6668	Bellatrix	γ Orionis	1.70	B2
6847	Mintaka	ϵ Ursae Majoris	1.68	A0
15145	Merak	β Ursae Majoris	2.44	A0
16268	Phekda	γ Ursae Majoris	2.54	A0
17518	Alioth	ϵ Ursae Majoris	1.68	A0
18643	Alkaid	η Ursae Majoris	1.91	B3
20947	Alphecca	α Coronae Borealis	2.31	A0
22193	Kornephoros	β Herculis	2.81	G8
*26161	Ascella	ζ Sagittarii	2.71	A2
Scanner flight 2				
519	Ankaa	α Phoenicis	2.44	G5
9188	Adara	ϵ Canis Majoris	1.63	B1
9443	Wezen	δ Canis Majoris	1.98	G3
9886	Aludra	η Canis Majoris	2.43	B5
13926	Regulus	α_1 Leonis	1.34	B7
*14177	Algieba	γ Leonis	2.61	K0
18643	Alkaid	η Ursae Majoris	1.91	B3
25466	Vega	α Lyrae	0.14	A1
30491	Deneb Algiedi	δ Capricorni	2.98	A5
32000	Fomalhaut	α Piscis Austrini	1.29	A2

*Double star.

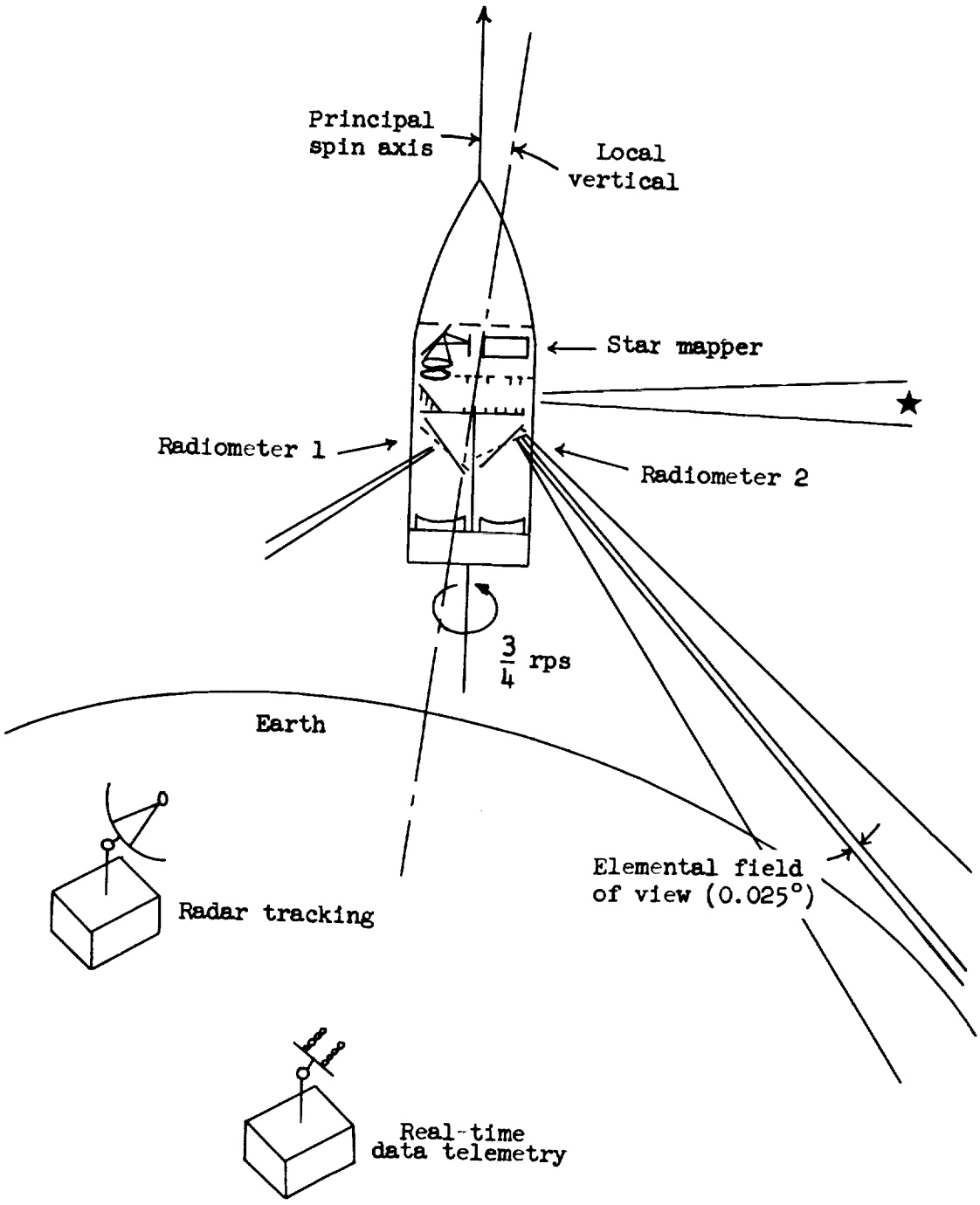

Figure 1.- Scanner spacecraft operational schematic.

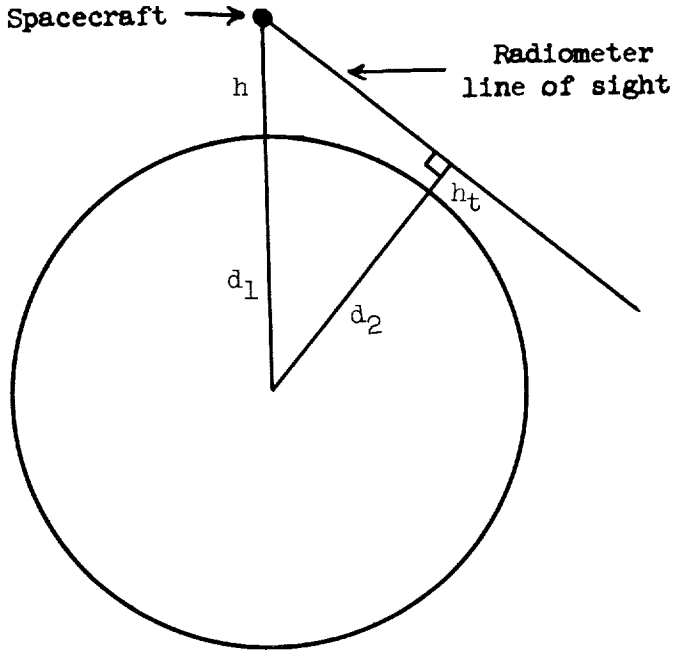

Figure 2.- Definition of tangent height, h_t.

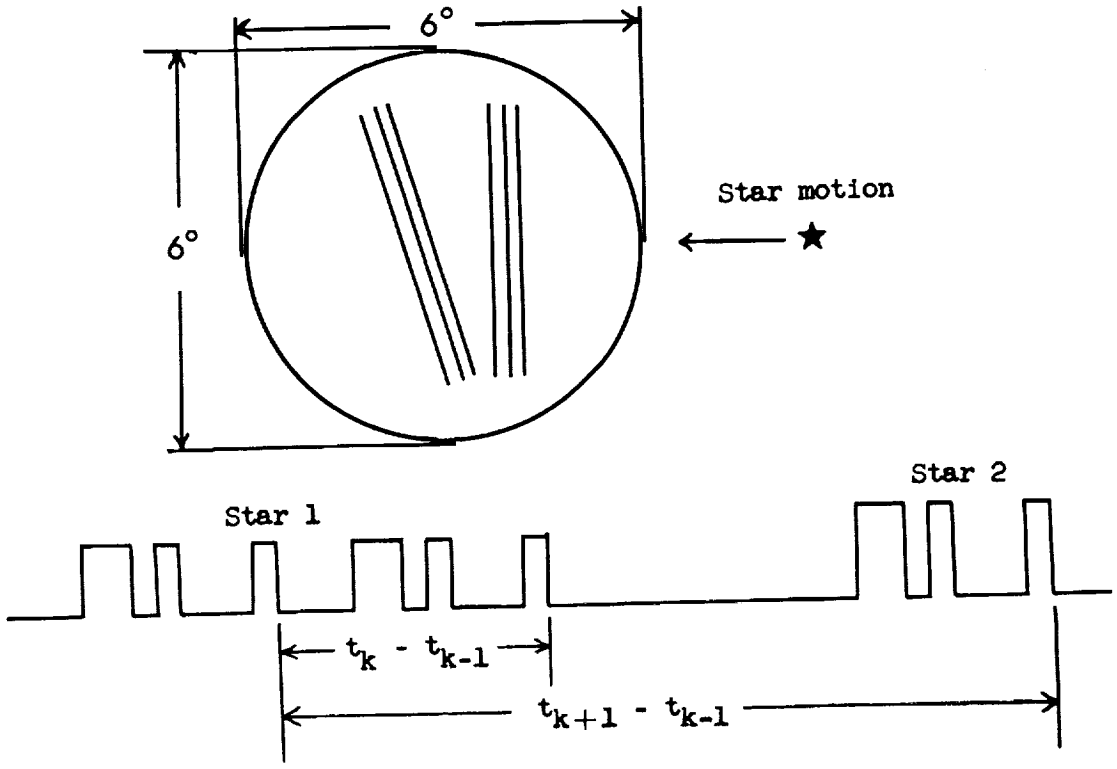

Figure 3.- Illustration of reticle and pulse groups generated by stars 1 and 2. Lines in reticle sketch represent transparent slits.

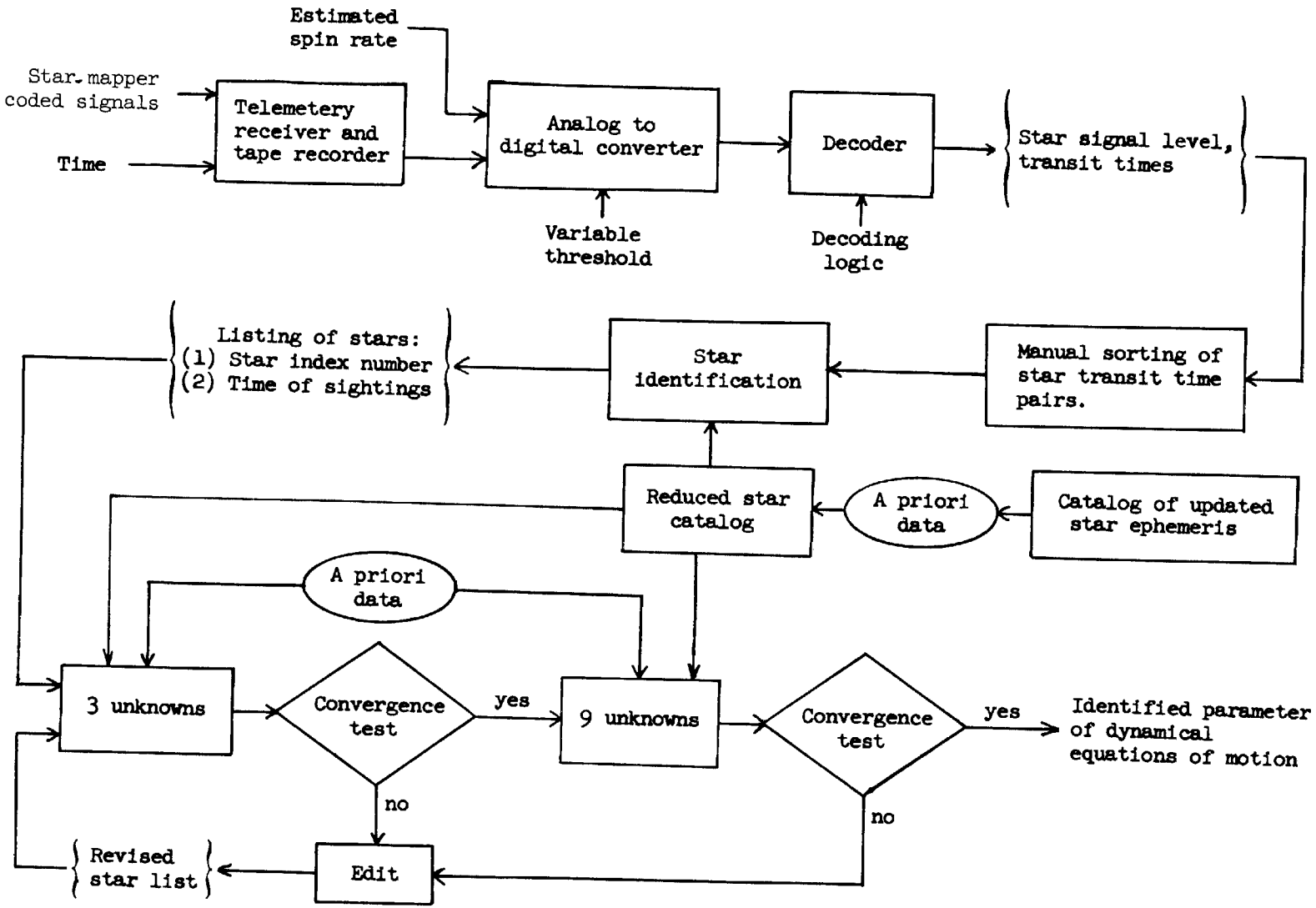

Figure 4.- Star-mapper data-processing procedure.

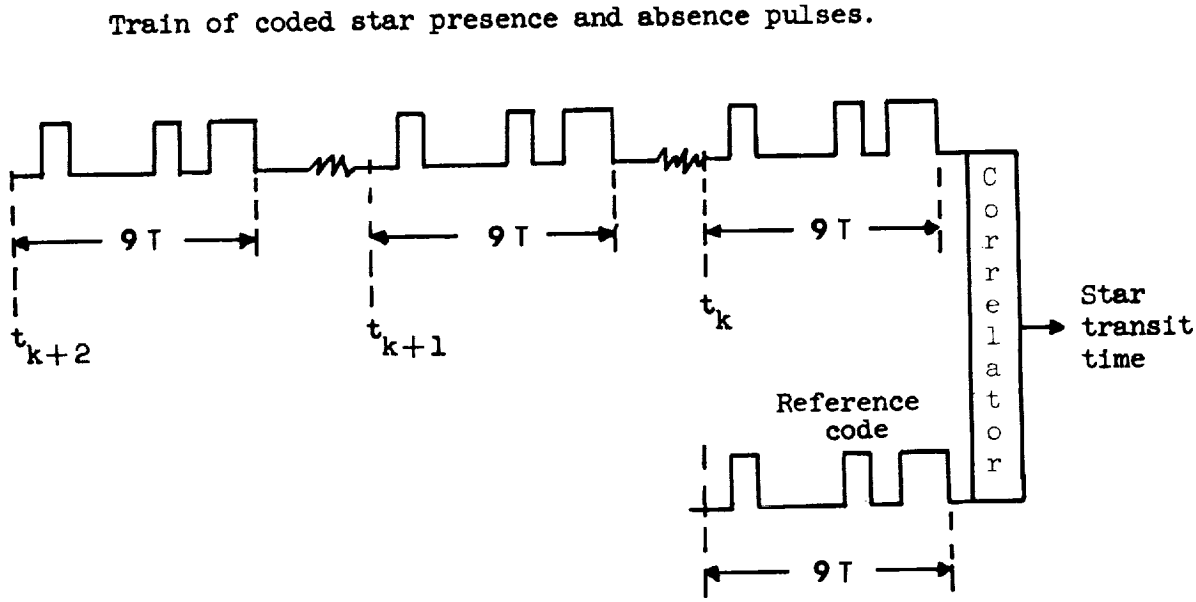

Figure 5.- Cross correlation of star-mapper pulse train with reference code group. Star-transit-time detection occurs at $t_k + \frac{T}{4}$ seconds.

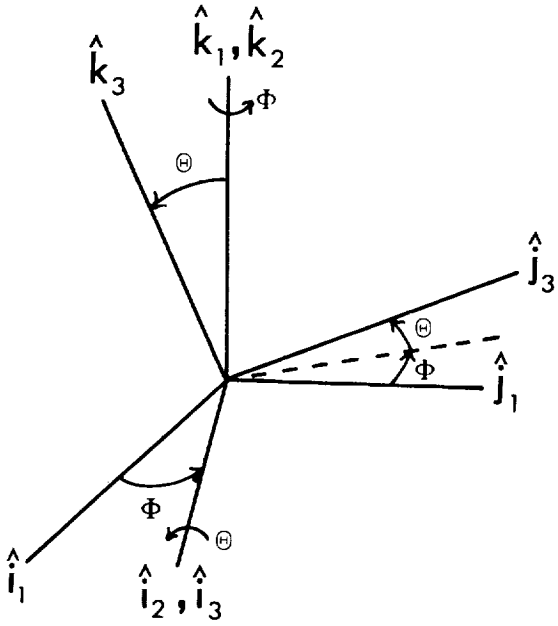

(a) Relationship of celestial and inertial reference frames.

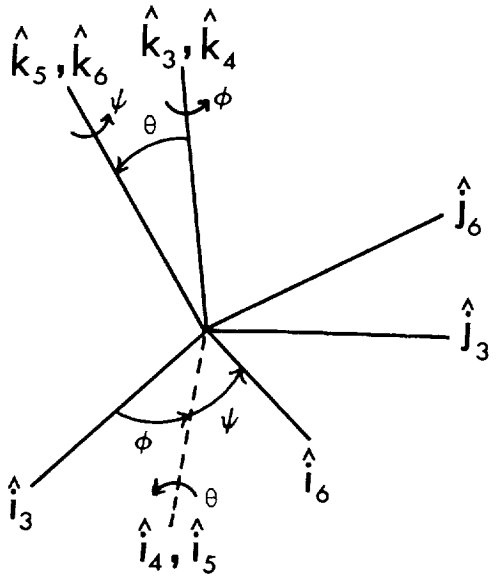

(b) Relationship of inertial reference frame to vehicle principal axes.

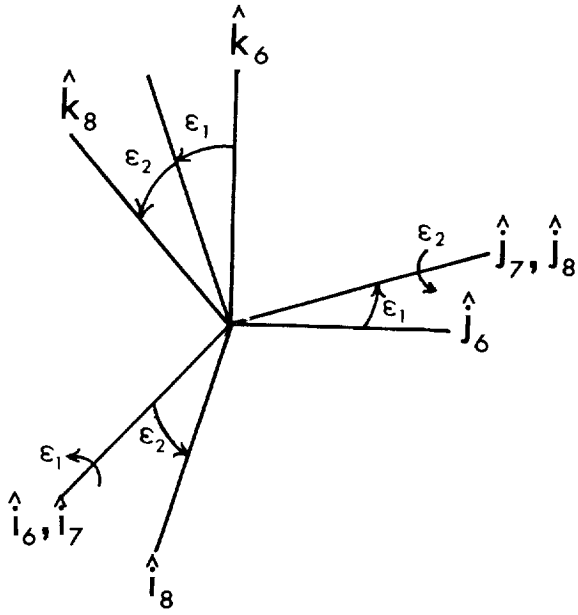

(c) Misalinement of vehicle principal axis with star-mapper reference frame.

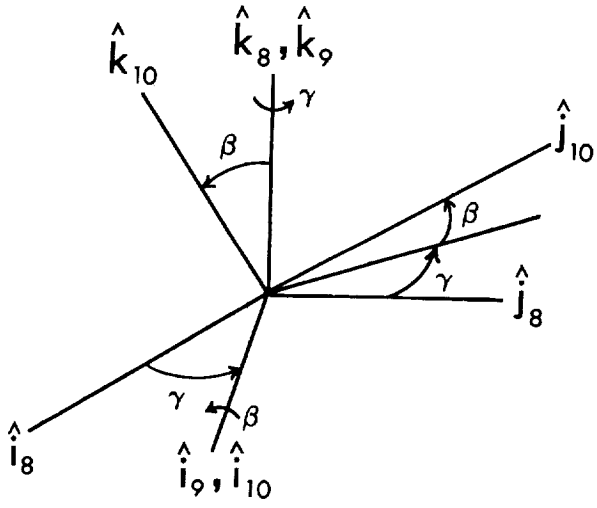

(d) Relationship of star-mapper reference frame to any slit plane reference frame.

Figure 6.- Basic reference frames of Scanner spacecraft-attitude geometry.

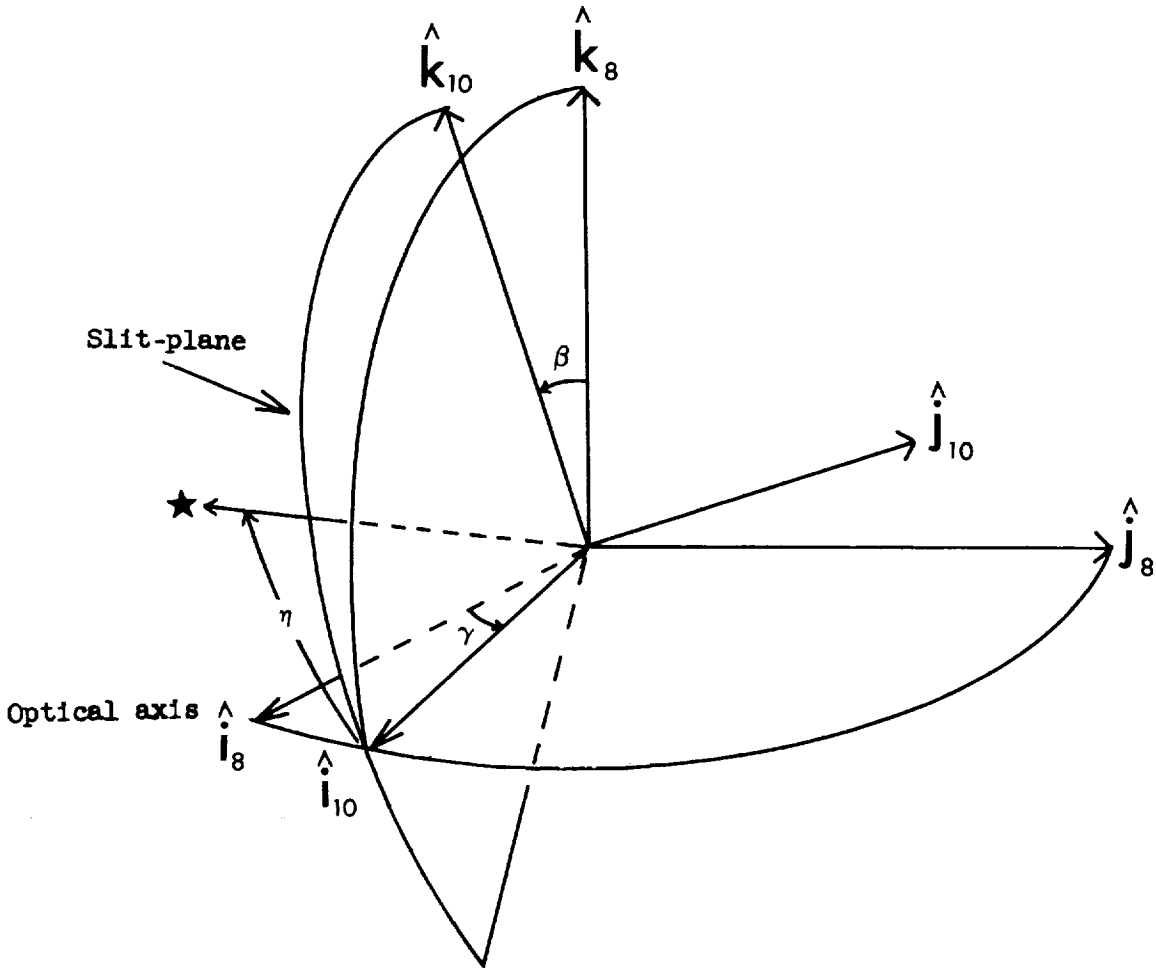

Figure 7.- Orientation of slit plane with respect to the star-mapper $\hat{i}_8$ - $\hat{j}_8$ plane.

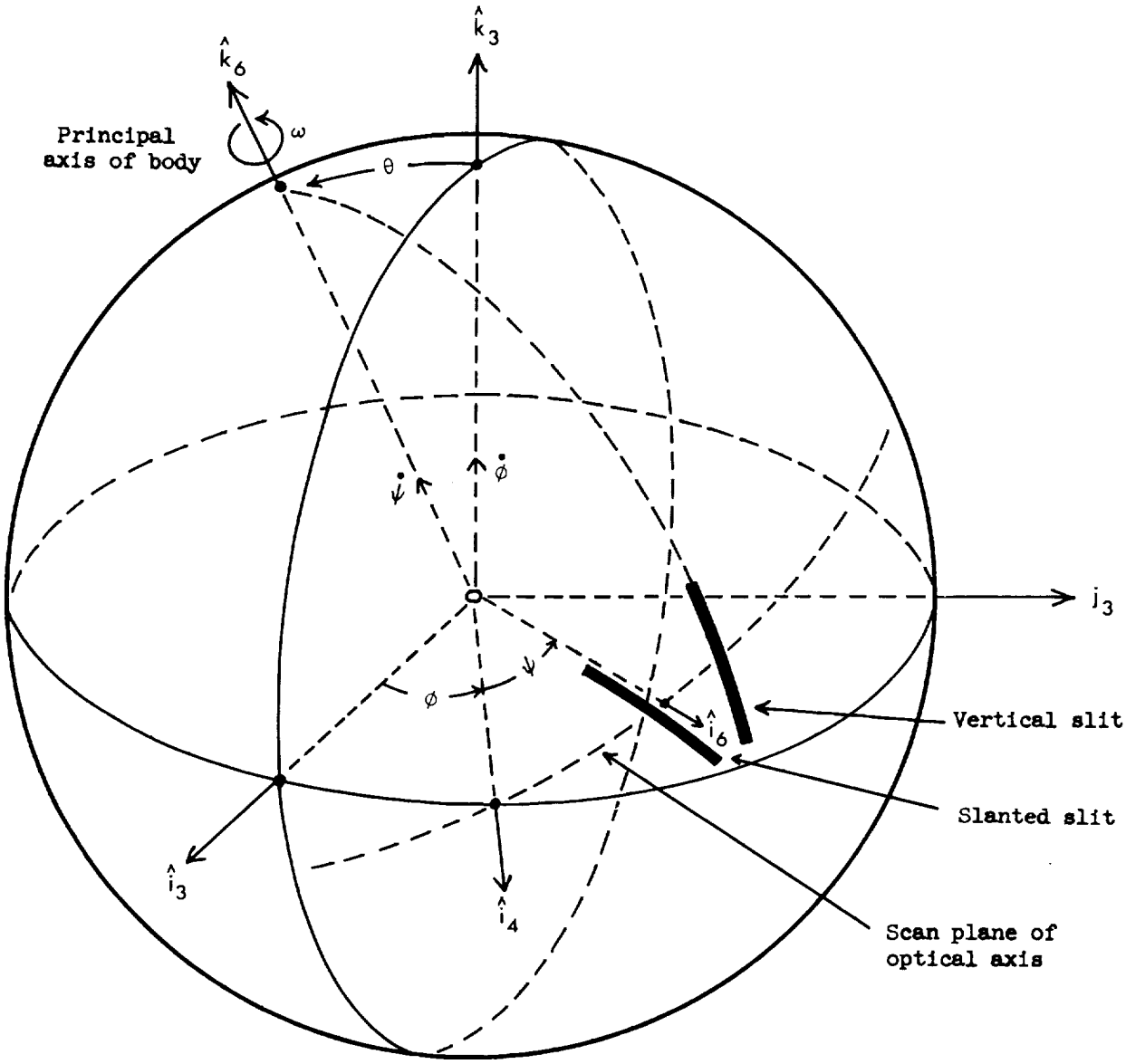

Figure 8.- Relationship of vehicle principal axes to inertial reference frame.

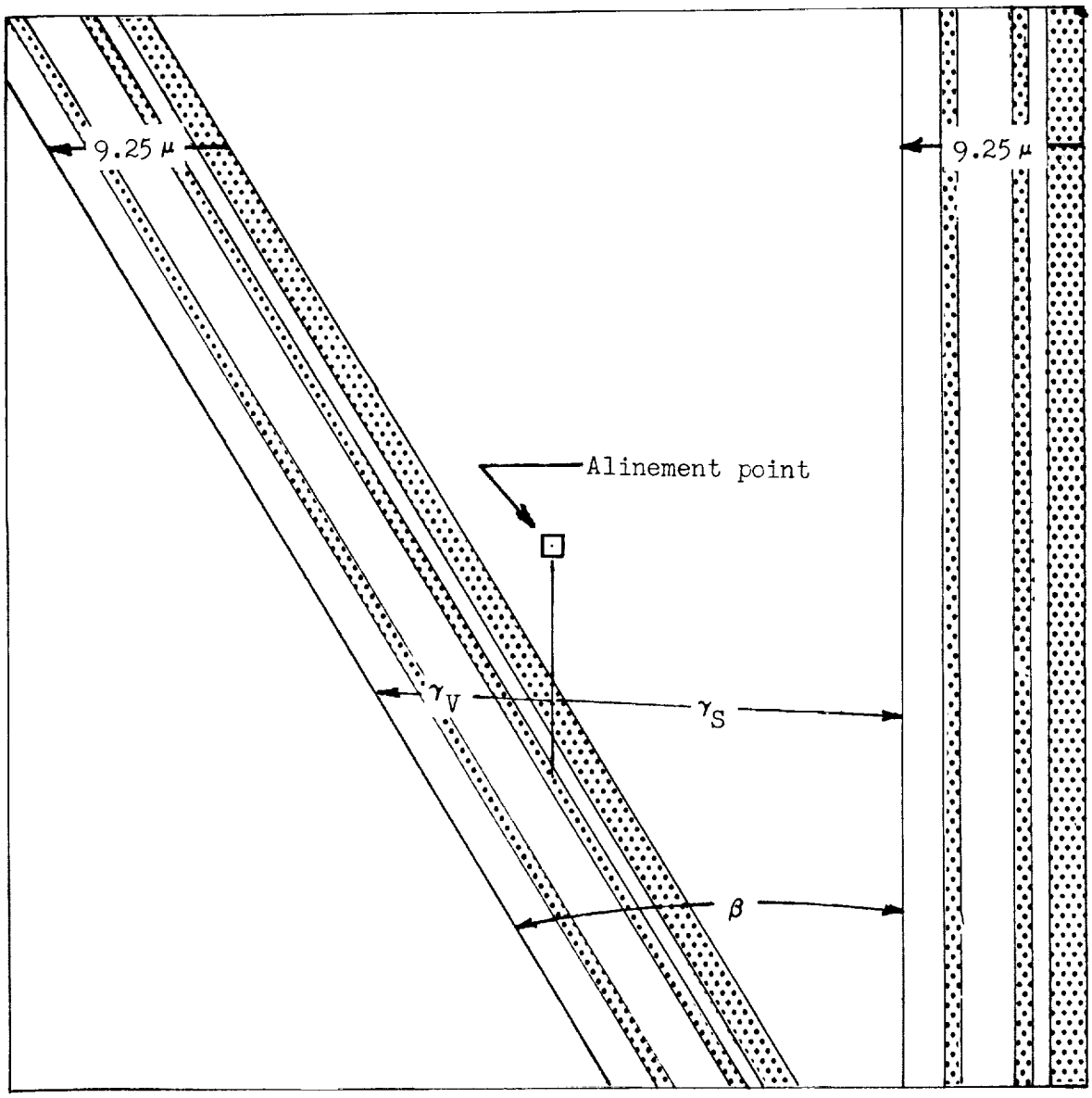

Figure 9.- Schematic of reticle showing the position on the reticle corresponding to the times recorded by data readout as a star's transit of a slit.

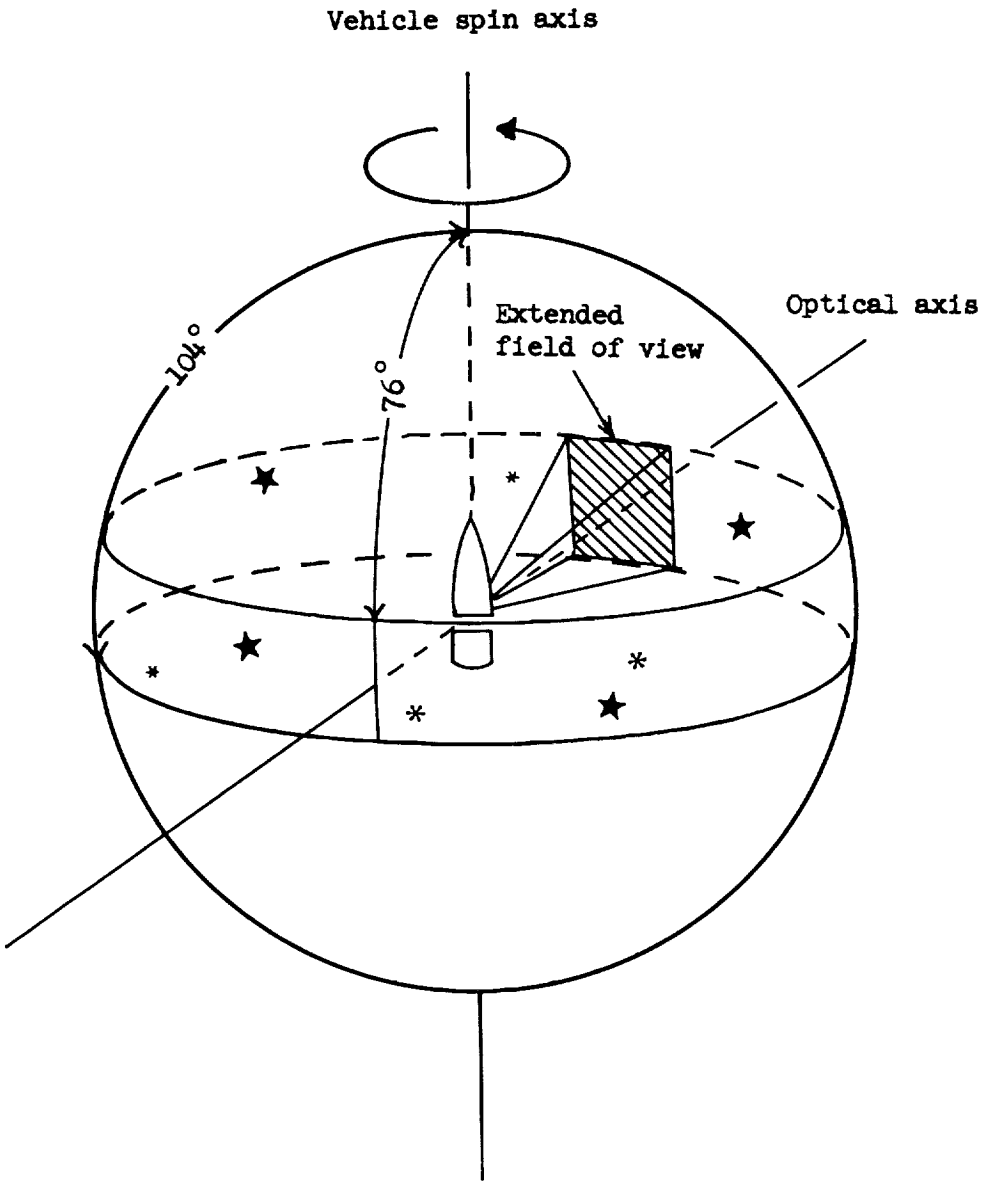

Figure 10.- Simplified scan of the star-mapper extended field of view about the celestial sphere for the case of zero cone angle.

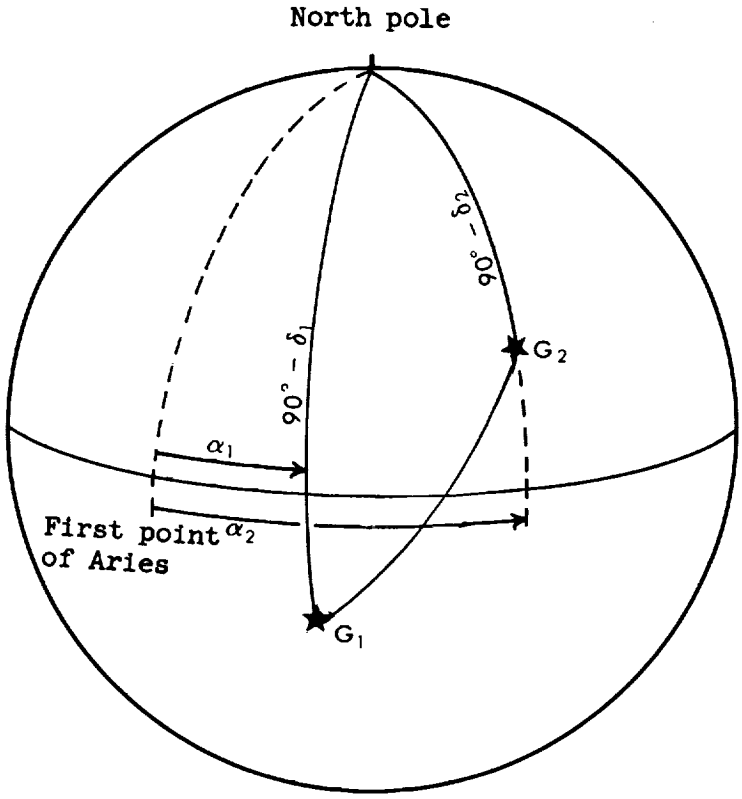

Figure 11.- Angular separation of two stars on celestial sphere.

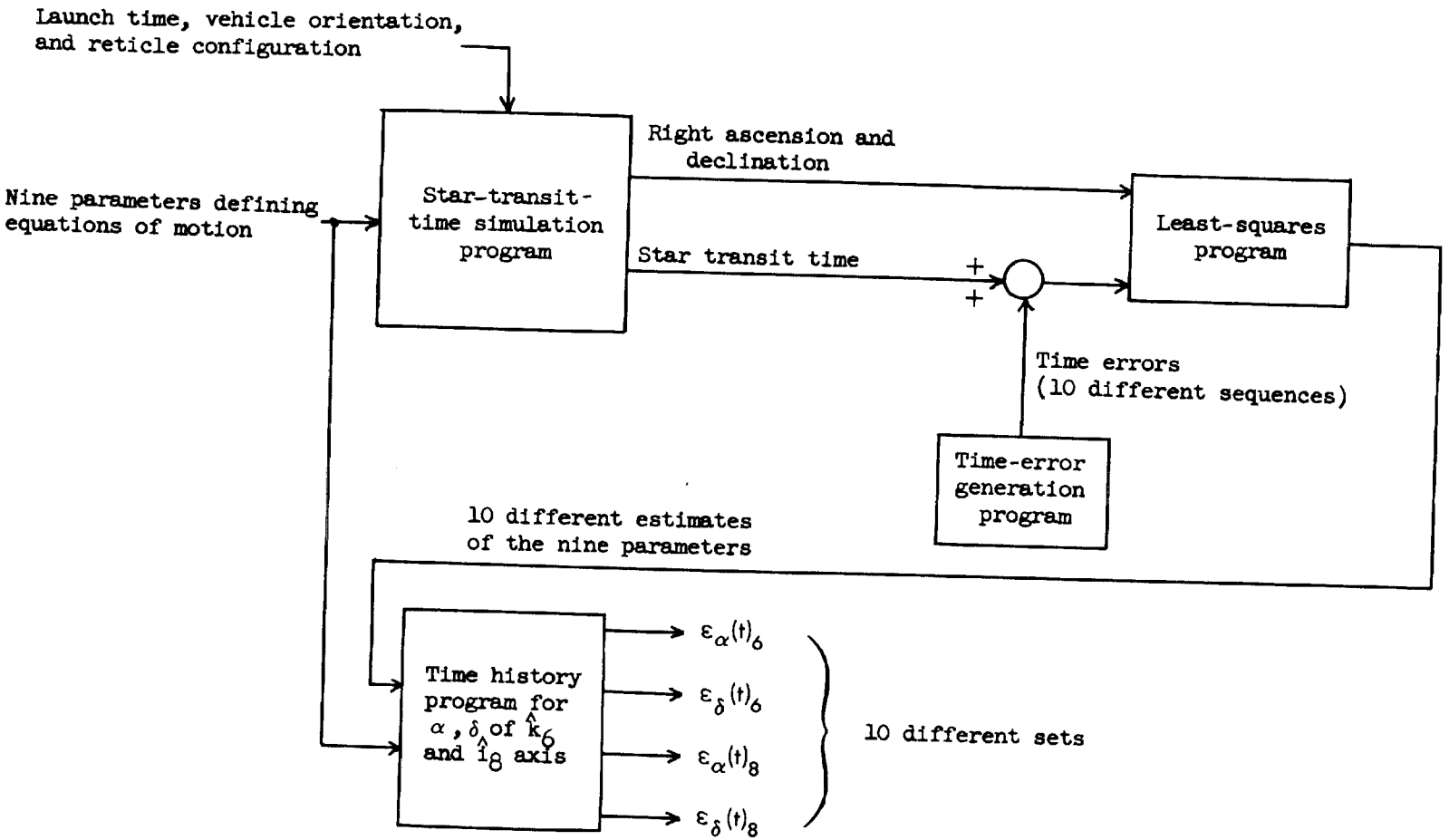

Figure 12.- Flow diagram of error-time-history generation.

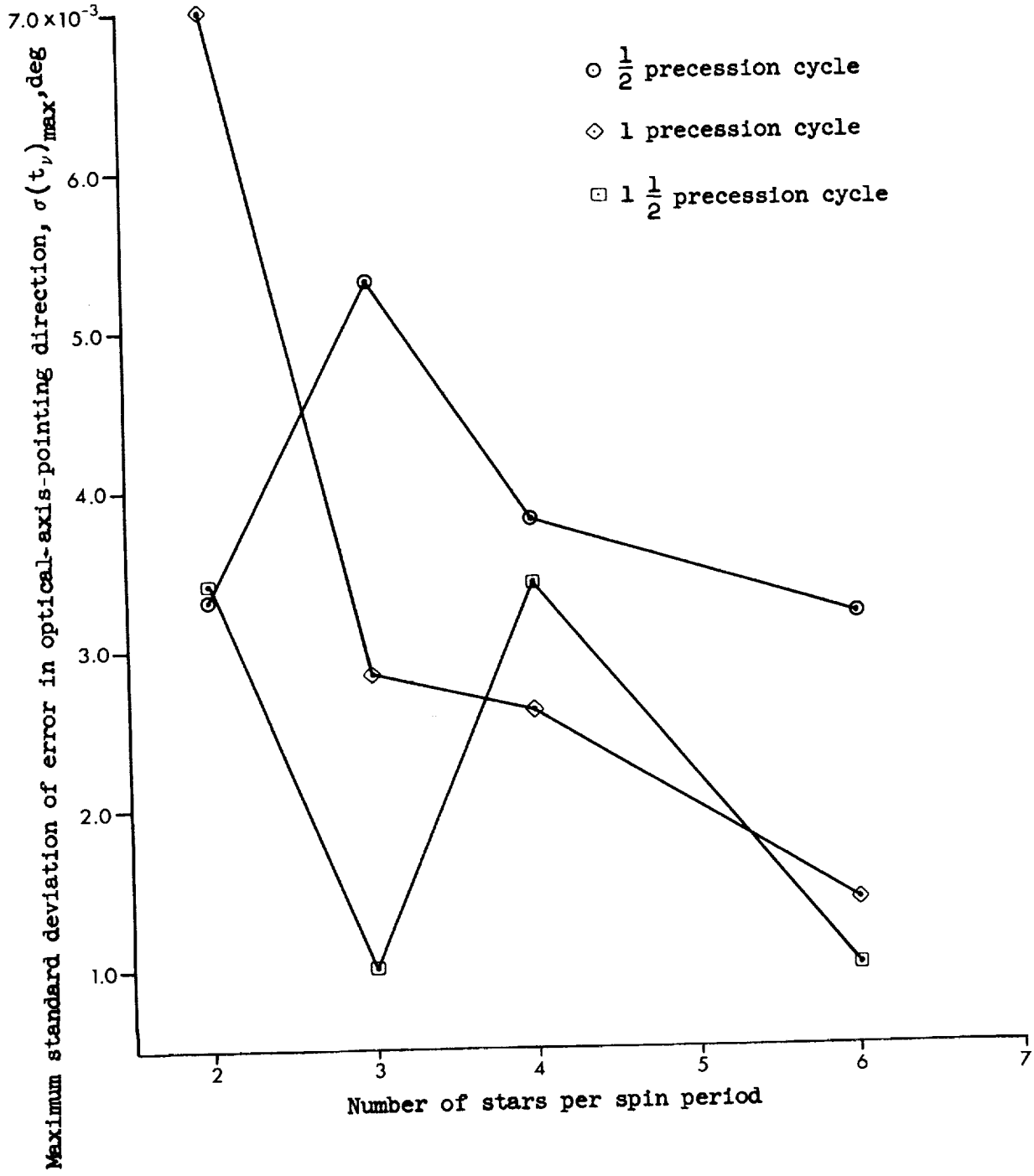

Figure 13.- Predicted standard deviation of pointing-direction error of star-mapper optical axis as a function of multiples of a precession cycle and number of stars per spin period.

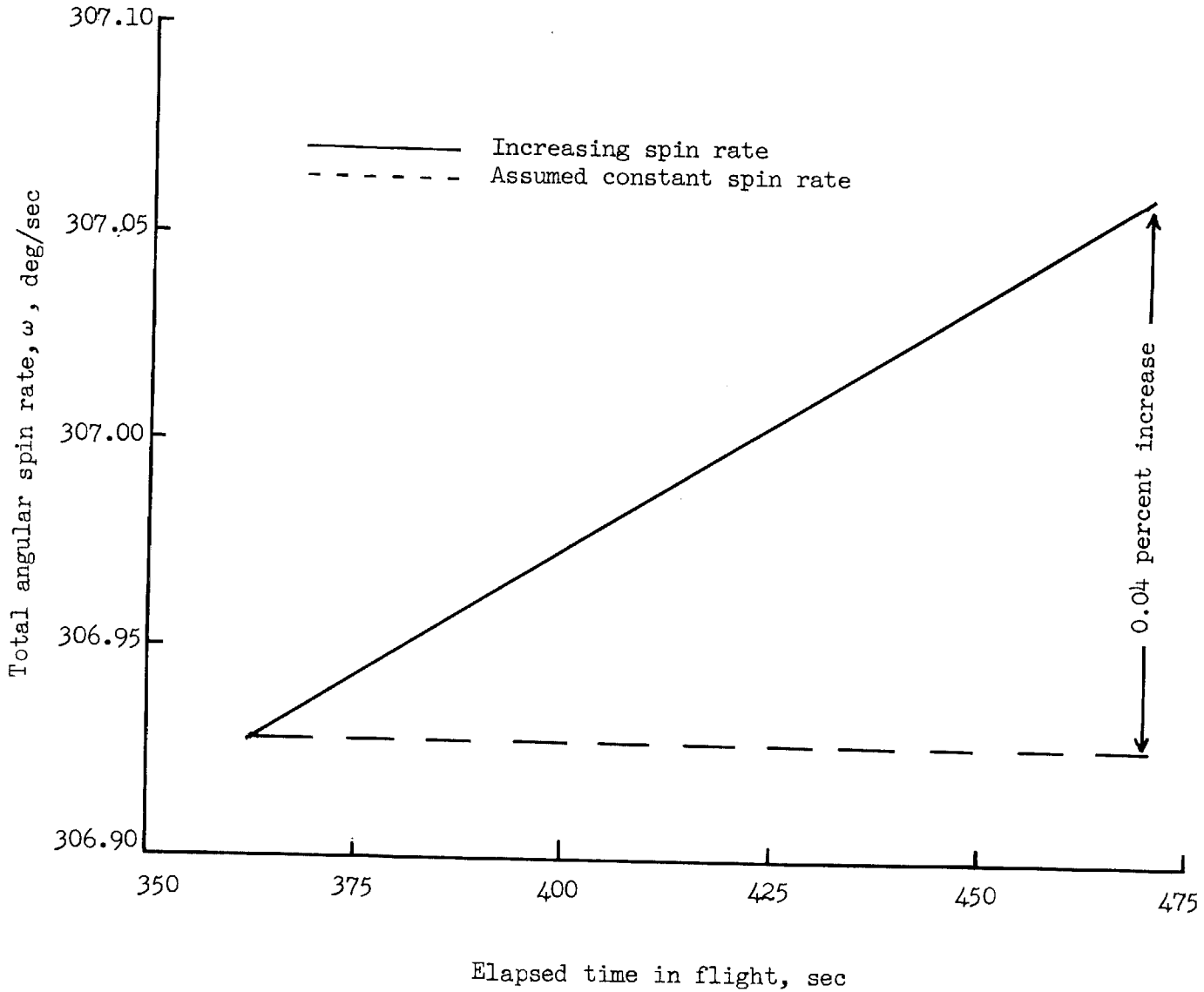

Figure 14.- Increase of total angular spin rate during the second data period of Scanner flight 1.

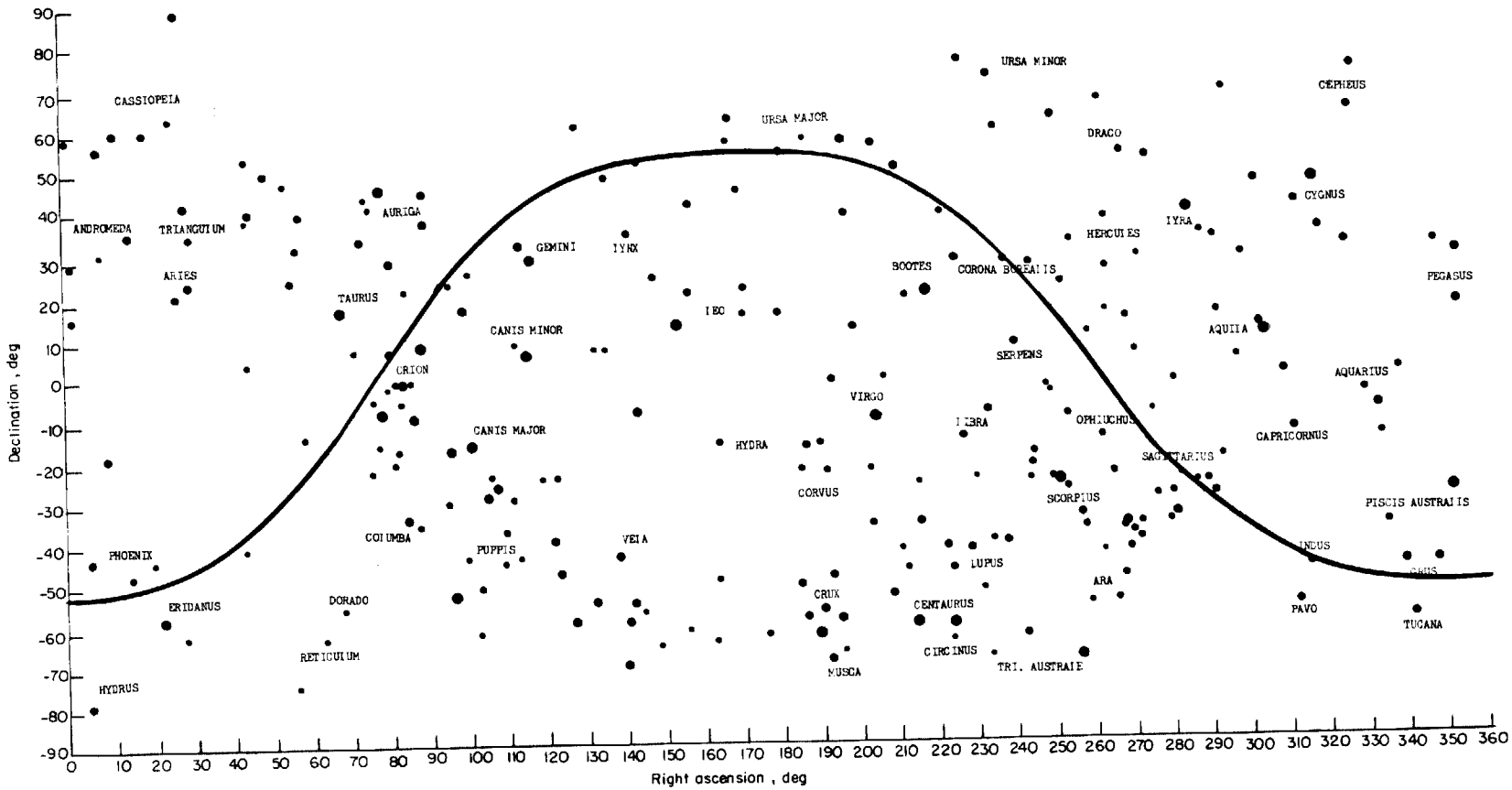

Figure 15.- Pointing direction of the star-mapper optical axis $(\hat{i}_8)$ for one vehicle spin period based on the set of nine vehicle motion parameters selected from the second data period of Project Scanner flight 1 for time beginning 6h 25m 46.7 s UT on August 16, 1966.

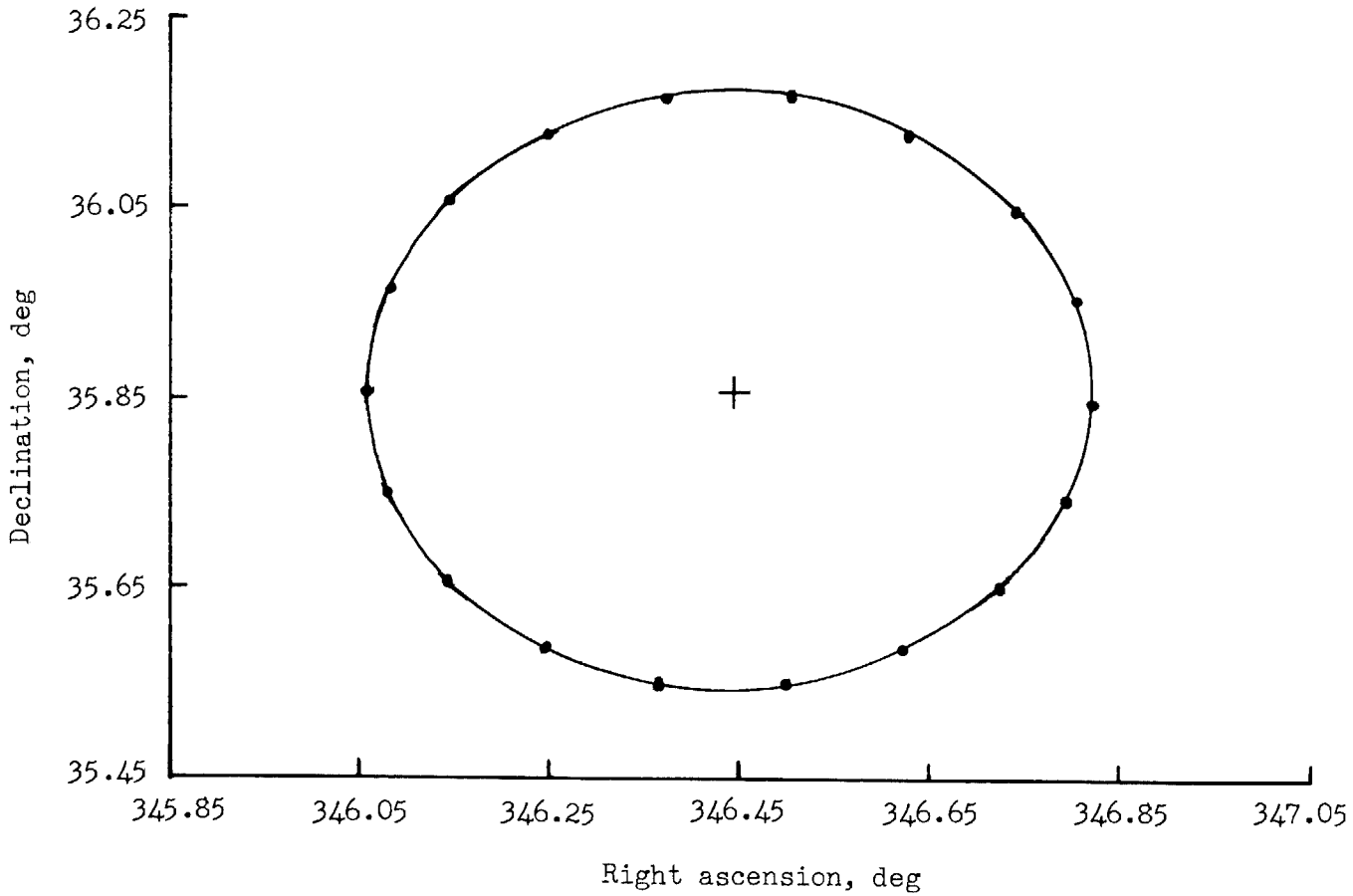

Figure 16.- Pointing direction of vehicle principal spin axis $\hat{k}_6$ for one precession cycle based on the set of nine vehicle motion parameters selected from the second data period of Project Scanner flight 1 for time beginning 6h 25m 46.7s UT on August 16, 1966.

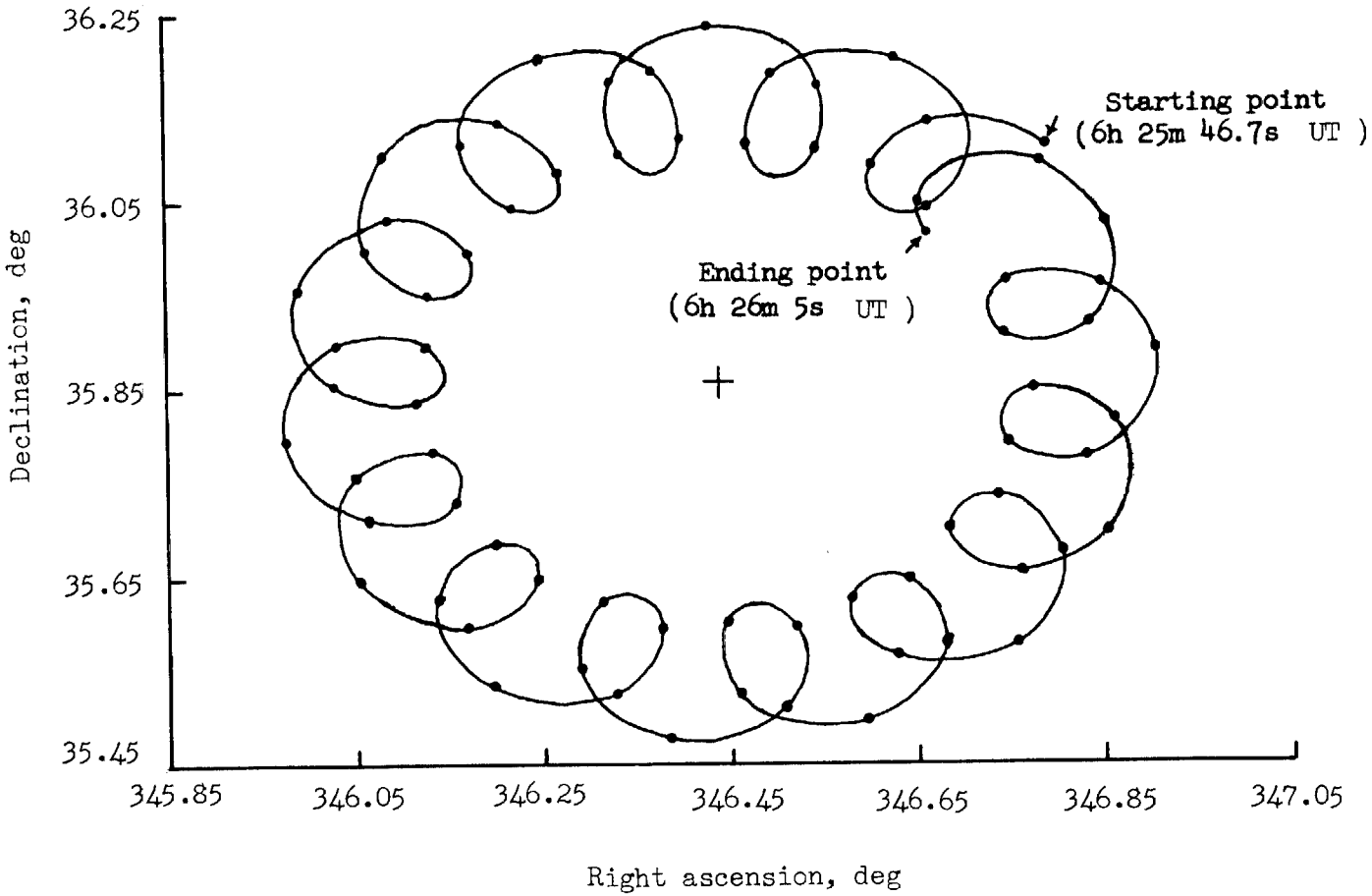

Figure 17.- Pointing direction of $\hat{k}_8$ axis for one precession cycle based on the set of nine vehicle motion parameters selected from the second data period of Project Scanner flight 1 for time beginning 6h 25m 46.7s UT on August 16, 1966.

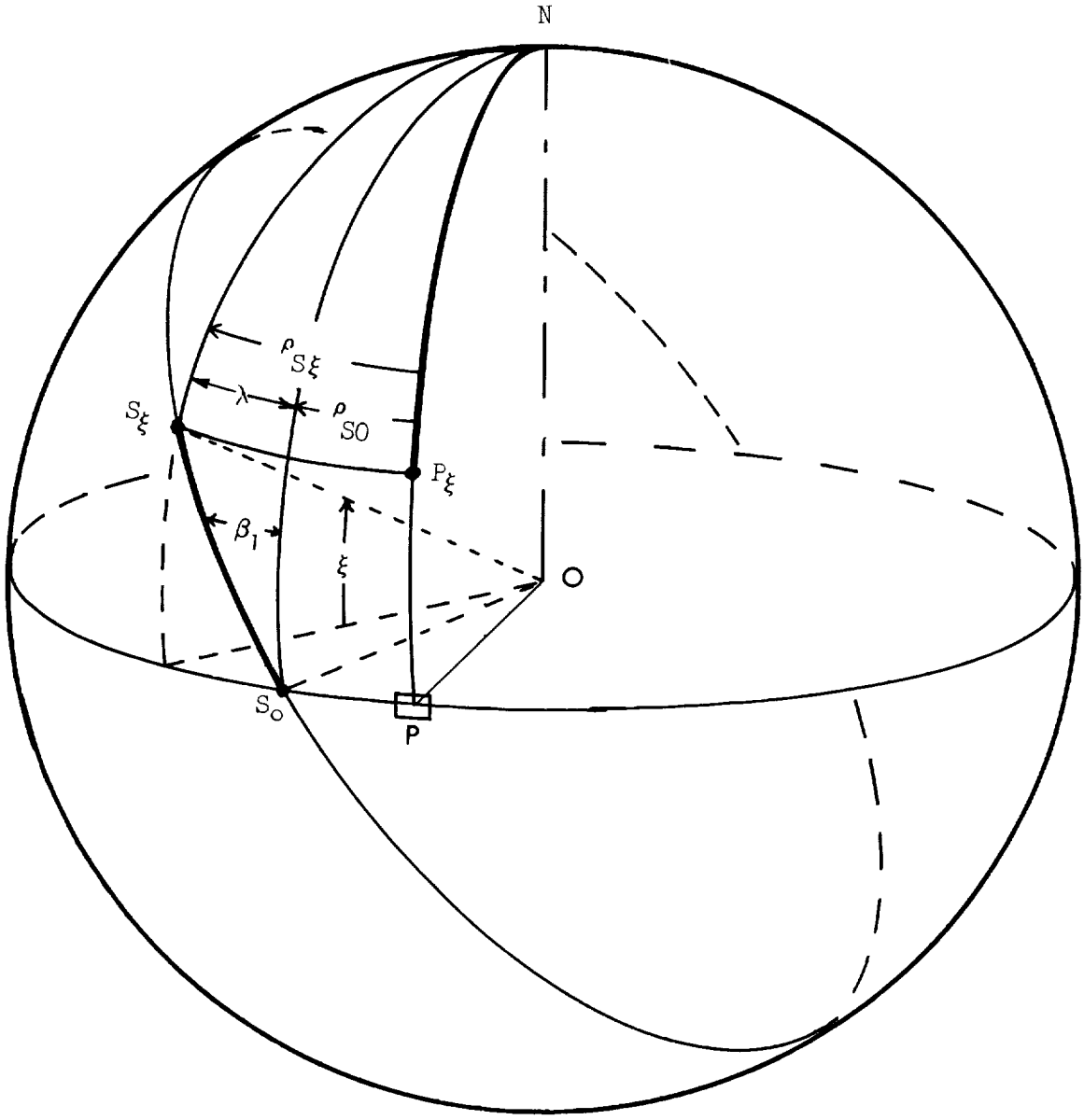

Figure 18.- Geometry of reticle measurements for the determination of β_1.